10.1098/rsta.2000.0689

THE ROYAL SOCIETY

Aircraft icing

By R. W. Gent, N. P. Dart and J. T. Cansdale

Defence Evaluation and Research Agency, Farnborough, Hampshire GU14 0LX, UK

This paper reviews the background to and the current status of analyses developed to address the problem of icing on aircraft. Methods for water droplet trajectory calculation, ice accretion prediction, aerodynamic performance degradation and an overview of ice protection system modelling are presented. The paper addresses the issues involved in the development of icing analyses including problem formulation and assumptions, solution techniques, validation and the incorporation of empirical inputs where a purely theoretical approach is not feasible. Results are presented to illustrate the capabilities of the analyses when applied to practical design problems. Recommendations are made for further research.

Keywords: icing; ice accretion; ice protection; aerodynamics; aircraft; modelling

1. Introduction

The protection of aircraft from the adverse effects of ice accretion has been a crucial design problem since the very early years of flight. In the 1940s and 1950s, significant experimental and flight test programmes laid the foundation for protection systems, the concepts of which are still in widespread use today. However, significant progress in theoretical studies of aircraft ice accretion was not achieved until the advent of the computer age in the late 1970s. The early works by Hardy (1946), Messinger (1953) and Langmuir & Blodgett (1946) represent an important foundation and early key milestones in the numerical analysis of aircraft icing. Without the advantage of modern computing devices, the early studies, though laying the mathematical foundations, were necessarily limited to geometries for which analytical solutions could be achieved, such as cylinders and spheres, or else relied on empirical solutions. It was not until the late 1970s that the theoretical research was focused on more representative geometries such as aerofoils and hence wings and helicopter rotors.

The main contributors in the resurgence of aircraft-icing analysis initially were NASA Lewis Research Center in the United States, and the Royal Aerospace Establishment (RAE), now the Defence Evaluation and Research Agency (DERA) in the UK. However, in the early 1980s the French research establishment, Office National d'Etudes et de Recherches Aérospatiales (ONERA), joined in what proved to be a very productive ten year period of tripartite collaborative research leading to the formation of the majority of the first generation icing analysis tools now widely used by aircraft manufacturers in the Western world.

Since the early 1990s, the number of agencies involved in aircraft-icing analysis has increased dramatically, with activities in Italy (CIRA), Spain, Germany and most notably Canada, who are now leading the way in the development of second generation analysis methods.

In very recent years, the foundations of aircraft-icing analysis have transformed the certification of aircraft for flight in icing from an almost total reliance on rig and flight test, to design by analysis for all new aircraft, with verification by rig and flight test. Analysis of aircraft icing previously deemed too difficult and complex a problem to analyse, has now taken its place in the modern world of aircraft design.

This paper describes the many varied types of analysis that have been developed for the study of aircraft icing and provides a record of the more significant findings to date. The physical processes of ice accretion are described in § 2, including the types of icing that may be encountered. The effects of ice accretion on aircraft are outlined in § 3, both for fixed-wing aircraft and for rotorcraft, for which the effects are materially different.

The traditional approach to aircraft-icing analysis begins with the determination of where and at what rate cloud water droplets impact the surface under analysis, say a wing. This requires a droplet trajectory analysis and the evaluation of the proportion of the free stream water concentration which impacts on the structure, referred to as the water catch or collection efficiency distribution. Analyses for this problem are described in § 4.

Once the water collection efficiency distribution is known, the analysis can proceed to determine how much and the location at which the impinging water will freeze. When this is known, the profile of the ice may be determined. The thermodynamic analysis required for the determination of ice accretion is described in § 5.

Ultimately, the aircraft designer wishes to know what effect the ice accretion will have on the performance of the aircraft. The strive towards ultra efficient propulsion systems in modern aircraft and the consequent reduction in the amount of engine bleed air available to provide ice protection for the lifting surfaces and the propulsion systems means that all modern aircraft must accept some ice accretion on tolerant areas as part of a design compromise. Typically, wing tips and roots may be left unprotected. The aircraft design engineer must demonstrate that the aircraft can tolerate such accretion safely and without undue performance penalty. In addition, the designer must demonstrate the ability for continued safe flight for a defined period in the event that the ice protection system has failed. Again, satisfactory handling qualities and performance must be demonstrated during this degraded mode of operation. The potentially vast range in the size and shape of ice accretions that may form means that empirical studies of performance degradation are not practical in isolation. Common practice is for the aircraft manufacturer to determine the most critical ice shape that may form on the aircraft in terms of the effect on performance and handling qualities. It is in this respect that ice-accretion analysis now plays a key role. The postulated 'worst case' ice profile is then usually evaluated via wind-tunnel tests and also frequently in flight test. However, progress in predicting the aerodynamic performance of clean aerofoils and wings has led to the potential for fully theoretical determination of iced aerofoil performance degradation. Progress in this challenging field is described in § 6. It is noted that determination of performance degradation is at a stage equivalent to that of the ice-accretion analysis in the early 1980s and therefore, despite much encouraging progress, considerable further work is required.

In § 7, a brief review is made of the analysis currently available for ice protection systems, both anti-icing and de-icing. Finally, § 8 makes recommendations for future research topics.

2. The problem

(*a*) *General*

This section describes the background to ice accretion, the basic physics of ice accretion and the types of ice that may form. The various forms of natural icing hazard are described.

(*b*) *Physics of ice accretion*

In order for the reader to become better able to understand the relevance and significance of the various icing and geometrical parameters, a basic introduction into the physics of ice accretion is described below. This is primarily intended for readers new to the field of icing.

Aircraft icing is defined as flight in cloud at temperatures at or below freezing when supercooled water droplets impinge and freeze on the unprotected areas on which they impact (hence the term 'impact icing' used in the BS 3G100 icing requirements). The rate and amount of ice accretion on an unheated surface depends on the shape, including surface finish,† the size, the speed at which the body is travelling, and the temperature, liquid water concentration (LWC) and the size of the droplets in the cloud.

It is convenient to consider accretion in two distinct parts. The first part is the rate at which the water droplets are intercepted by the body. This is the product of the efficiency that the body collects the water (usually referred to as the water droplet collection or catch efficiency), the amount of water contained in the cloud (the cloud LWC) and the speed of the body through the cloud. The water droplet collection efficiency of the body is controlled mainly by the size (e.g. rotor blade chord length) and the shape of the body, including the incidence, and, in particular, the diameter of the cloud droplets. While airspeed is important also, the ambient pressure (altitude) and temperature have only a limited effect on the collection efficiency over the range of values appropriate to aircraft.

The second aspect to ice accretion is the rate at which the impinging water will freeze to form an ice accretion. This is primarily governed by the heat transfer from the surface of the body. This heat transfer includes kinetic heating, convective cooling, evaporative cooling, latent heat of freezing and a number of smaller contributions from sensible heating and cooling mechanisms. For the impacting water droplets to freeze, their latent heat of fusion must be dissipated. The primary mechanisms of heat loss are normally convection and evaporation. The convective heat transfer is in practice largely controlled by the geometry and speed of the body in the airflow, the roughness of the iced surface and the ambient temperature difference that exists between the surface and the local air temperature (edge of boundary layer under compressible flow conditions). The evaporative cooling is a function of the vapour pressure of the water, which is itself a function of the temperature and the pressure at the surface. The pressure effect is through the enhanced concentration gradient that exists if the air is expanded and cooled, as in the upper surface suction region of an aerofoil or within an engine inlet.

† Very small discontinuities on a smooth surface, such as dents, rivet heads and poorly aligned panel edges, can promote considerable ice growth on surfaces and in areas that would otherwise remain substantially ice free.

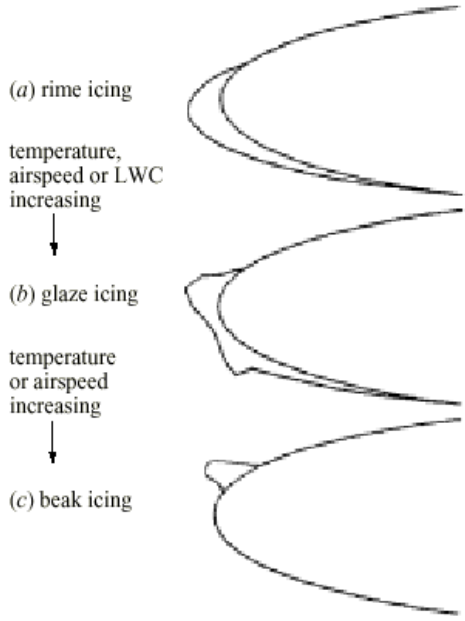

Figure 1. Main types of ice accretion which may form on a wing/rotor blade.

When a forward-facing component of an aircraft such as a wing leading edge passes through the supercooled droplet cloud, the impinging droplets will try to release their latent and freeze to form an ice accretion.

If the droplets freeze completely on impact, they tend to form a white opaque accretion which is relatively streamlined, but with a surface roughness much greater than that of the wing or other component on which they form. This type of accretion is termed *rime* ice (figure 1*a*). It tends to form at combinations of low ambient temperature, low speed (low kinetic heating) and/or a low value of cloud water concentration. If the icing encounter is particularly long, and/or if the collection efficiency is large leading to a relatively large accretion, the rime ice profile may become less streamlined and can sometimes take on the form of a pointed or 'spearhead' appearance.

At combinations of warm temperature (i.e. close to freezing), high speed or high cloud water concentration, not all of the impinging water freezes on impact, the remainder running aft along the surface. It is possible for this so-called 'runback' water to freeze at aft locations, producing localized thickening of the ice profile into what appears to be a horn on each of the upper and lower surface in the case of a wing. This accretion tends to be translucent in appearance and is termed '*glaze*' ice (figure 1*b*). The surface roughness of glaze ice accretion can range from fractions of a millimetre up to localized three-dimensional nodules several millimetres in height and width. At transitional conditions between rime and the very wet glaze accretions, it is possible for the translucent region to be confined to a narrow band close to the airflow stagnation point of the wing, with the accretion aft becoming opaque and white in appearance like rime ice. Some researchers term this intermediate stage of ice accretion '*glime*' ice, although this is not a preferred definition by the authors.

Finally, at warm temperatures and/or high speed, such as exists in the tip region of a helicopter rotor in flight, the only place conducive to ice accretion is in the low-pressure (suction) region on the upper surface of the aerofoil close to the leading edge, where cooling due to adiabatic expansion mitigates the effect of kinetic heating. A slushy ride of ice termed '*beak*' ice (figure 1*c*) is observed to form. If the icing cloud is vacated, or if the lift is reduced say during a descent, the ridge of ice sheds very quickly. Such accretions can be readily simulated in icing wind-tunnel tests, and on rare occasions have actually been photographed during flight. They tend to be self limiting in size since their presence disrupts the aerodynamic flow and hence the suction needed for ice formation.

Due to the variation in the local velocity with span along a helicopter rotor, it is possible for all three types of accretion to be present at the same time. Rime ice can form on inboard stations, glaze ice further outboard and beak ice on the outboard span of the rotor. However, on other components such as the fuselage or stabilizer, or the wings of a fixed-wing aircraft, the accretion will, in general, be of either rime or glaze ice type or a combination of both.

One final point to note is the change in the temperature of a surface during the initial period of icing, the direction of which varies depending on the total air temperature. If the total air temperature is below zero, then the convective and evaporative cooling mechanisms combine to dissipate the latent heat of the supercooled droplets and this maximizes the rate of accretion. The temperature of the accreting surface in this icing condition will tend to *rise* due to the release of latent heat and will be at the freezing point if the accretion is particularly wet. On the other hand, if the total temperature is positive due to kinetic heating (i.e. in the region of a rotor tip), the only 'cooling' mechanism is likely to be evaporation. Under these conditions, the surface temperature will *fall* to zero and hence ice may accrete.

(*c*) *Icing parameters*

(i) *General*

This section discusses the various parameters which influence the severity of the icing condition. The parameters discussed include both the icing conditions (outside air temperature, volume median diameter and the LWC) as well as certain other flight and atmospheric conditions (airspeed and altitude) which can contribute to the severity of the condition as experienced by the aircraft.

Ice accretion from supercooled water droplet clouds represents only one form of a number of natural hazards to the aircraft. Though the classical supercooled cloud may exist by itself, it is also likely that the aircraft will encounter other forms of ice-producing precipitation. Any icing clearance will need to address the hazards posed by snow, ice crystals and supercooled water both in isolation and in appropriate combinations. In practice, these forms of natural hazard are closely related. While the physics of ice nucleation is somewhat complex and outside the scope of the present document, a brief description is considered to be useful. Readers are referred to Mason (1971) for a more in detailed explanation.

In practice, water droplets will condense on soluble nuclei to form a cloud. Due to their relatively small size, cloud droplets may frequently exist in the supercooled state down to −20 °C and, less frequently, as low as −30 to −35 °C. For very small droplets of a few micrometres diameter, water droplets have been observed in the laboratory

to remain supercooled down to −40 °C (see Mason 1971). However, at temperatures below this, the droplet will freeze spontaneously. The degree of supercooling at temperatures above −40 °C depends on the purity of the water, the size of the droplets and whether ice particles are already present in the cloud. If ice particles are present then they will grow at the expense of the water droplets, which rapidly evaporate. Also, if supercooled water droplets collide with ice particles or other ice nuclei, the water droplets will freeze. It is important therefore to note that as the ambient temperature reduces, the likelihood of large supercooled water droplets will reduce. In consequence, therefore, freezing rain, which is effectively supercooled cloud with very large droplets (up to *ca.* 5 mm diameter), is unlikely to exist at cold temperatures (below −20 °C). This feature is supported by the observation that this is a relatively warm-temperature phenomenon. Since the droplets are associated with precipitation, it is possible to encounter freezing rain at temperatures above 0 °C.† A typical guideline for the temperature band appropriate to freezing rain is +5 to −15 °C.

Freezing rain differs from freezing drizzle in terms of the diameter of the droplets and the processes by which the droplets form. Most precipitation in mid-latitudes is initiated with glaciation of clouds. Snow which forms within these clouds falls through the warmer lower layers of the atmosphere and melts to form large rain droplets (greater than 400 μm in size). If these droplets once more fall through a sub-freezing layer, which can be associated with an inversion layer, they can become supercooled and freeze on contact with a surface. This is generally referred to as freezing rain. Freezing drizzle is expected to consist of droplets with diameters typically in the range 50–400 μm and is associated with stratoform cloud of relatively small vertical extent which forms in sub-freezing temperatures. The drizzle size droplets are produced by coalescence which can be enhanced by turbulence induced collisions near the cloud top but, because of the small cloud depth, these fall out of the cloud before they can grow to larger raindrop sizes. The maximum water concentration is expected to be relatively low in the range 0.3–0.4 g m^{-3}.

Ice crystals may grow in an ice supersaturated environment by sublimation of water vapour to their growing surface. As the equilibrium saturated vapour pressure over ice is lower than over water, once glaciation is initiated in a supercooled water droplet cloud, the cloud will quickly transform into an ice crystal cloud. The ice crystals may aggregate to form a snowflake and the snowflakes may themselves collect supercooled water. Depending on the conditions, therefore, the crystalline particles may range from pure ('dry') ice crystals through to large melting ('wet') snowflakes. The hazard that the ice crystals represent to the aircraft will be different, as will the hazard to individual components. For instance, pure ice crystals are unlikely to accrete on the rotor of a helicopter, having a tendency to bounce off the surface, whereas in sufficient quantities, the ice crystals may collect in an intake plenum chamber and hence represent a hazard to the engines. Furthermore, such crystals may produce a hazardous accretion, slush or ice, if captured by a wet surface, produced possibly

† Freezing rain is normally associated with frontal conditions where temperature inversions exist. Ice accretion on an airframe exposed to freezing rain or drizzle may be produced by one of two mechanisms. The first, and most likely, is precipitation (such as snow) that has fallen through or from a positive temperature layer into a sub-zero level, where the resulting large droplets have been cooled and then impinged and accreted upon a cold surface. The second is a transient condition associated with an aircraft that has climbed or descended into positive air, where rain of positive or negative temperature accretes for a period upon a cold soaked airframe; this latter condition is unlikely to produce any rotor blade icing and therefore tends to be a fixed-wing aircraft problem.

by a heated or fluid anti-iced surface. Water running from such melted crystals or snowflakes may run to colder unprotected areas of the airframe and form unwanted hazardous ice accretions.

In this document, only a relatively brief and superficial review of icing hazards is presented with the attempt made only to convey the more significant aspects as perceived by the authors. Further information is provided on each of the parameters affecting ice accretion in the following paragraphs. Examples of the ranges and typical values found in nature are also provided, where appropriate, for information.

(ii) *Outside air temperature (OAT)*

By far the most critical parameter influencing the accretion of ice from supercooled cloud is the ambient (outside) air temperature. While the static temperature of the air is important to ice accretion, and is relatively easily measured and therefore available to the pilot, it represents only one part of the accretion physics. In practice, it is the surface temperature of the body which dictates whether accretion is possible and the rate at which this accretion proceeds. Clearly, with a thermal protection system fitted, the aim is to raise the temperature of the surface above zero, either on a temporary basis (de-icing) or on a permanent basis (anti-icing). For an unheated and thermally isolated surface, the total temperature is the more relevant parameter to the rate of ice accretion. For instance, the tips of a rotor blade experience considerable kinetic heating. Simple analysis suggests that the tip of a rotor on a typical conventional helicopter, near the stagnation airflow position, will be *ca.* 20–25 °C warmer than the root of the blade. Heat conduction within the blade will reduce the temperature rise that is achieved in practice. It is the kinetic heating in the outboard section of the rotor which makes a limited helicopter icing clearance (without rotor protection) feasible. In practice, kinetic heating will prevent or reduce the susceptibility of the rotor to icing, and consequent performance degradation, when operating at ambient static air temperatures in the region between 0 and −10 °C. As the OAT reduces, the potential and the extent of the ice along the span of the rotor will increase. As ice forms further outboard on a rotor when the ambient temperature is reduced, so the performance degradation caused by the ice accretion will increase. Similarly, military fast-jet aircraft rarely have wing ice protection systems, since they have the option to accelerate to an 'ice-free' airspeed. The same therefore tends to apply to any aircraft travelling at high speed (e.g. Mach number not less than 0.6). On the other hand, while civil transport aircraft may cruise normally at high subsonic Mach numbers and hence avoid significant risk of icing, they must be protected for low-speed climb and, particularly, descent through cloud where the constraints in controlled airspace limit such ice avoidance strategies, e.g. flight in a holding pattern.

In terms of the accretion process, the OAT controls the degree of convective cooling available and hence the dissipation of the latent heat released from impinging supercooled water droplets. Hence, the lower the OAT, the higher the potential for convective cooling, and the greater tendency to freeze any impinging water. For wings and other external flow components, the important temperature range is from freezing to *ca.* −30 °C. However, for engine intakes, it is possible for a venturi process to exist under certain conditions (e.g. engine running on the ground), such that a local temperature depression can exist inside the intake. For this region, the design

of engine ice protection systems will normally consider OAT values up to *ca.* +5 °C. (Although, for hot-air ice-protection systems, higher values usually have to be considered in terms of ensuring that structural integrity is retained should the air anti-icing valve fall open during take-off on a hot day (+45 °C). However, this is not strictly an ice-accretion design point and does not therefore need to be considered further in this article.)

A secondary but important effect of OAT is the link between droplet size and the degree of supercooling which can exist. As the OAT is reduced, the probability of encountering large amounts of supercooled water droplets (i.e. high LWC) is also reduced. Design atmospheres for use in aircraft ice protection certification reflect the trend in nature between OAT and LWC. In the civil requirements (e.g. FAR 25, appendix C) or the UK military design requirements (see Ministry of Defence reports DEF STD 00-970 (1994) and 00-971 (1987)), the maximum continuous value of LWC that may be encountered is 0.8 g m^{-3} at 0 °C. This is associated with stratoform clouds. At −30 °C, the maximum LWC likely to be encountered in stratoform cloud reduces to 0.2 g m^{-3}. The value of LWC is higher for cumuloform clouds, although a similar trend with OAT exists.

It is important to note that the occurrence of a total temperature greater than 0 °C alone at the surface of a body (fuselage and, in particular, the rotor) in clear air is not a valid criterion for the prevention of ice accretion on a body in supercooled cloud. Evaporative cooling will drive the surface temperature of the body to the freezing point and, under appropriate conditions, will lead to ice formation. The rotor is again a prime example. The degree of evaporative cooling is affected by the surface pressure of the body. While the outboard region of a rotor in clear air may be at a temperature above the freezing point, the presence of impacting cloud water droplets will drive the surface temperature to zero due to evaporative cooling. This is particularly true in the low-pressure region on the upper surface of a rotor, where the combined effects of adiabatic expansion and enhanced evaporative cooling can lead to the formation of a beak ice accretion, as defined earlier.

In contrast, however, the kinetic heating on a helicopter fuselage or low-speed aircraft is small (less than 2.5 °C maximum at 140 knots). Hence the static air temperature provides a reasonable guide to the likelihood that ice will accrete on the fuselage and other components mounted on the fuselage. In the absence of external heat sources, therefore, the colder the air temperature, the greater the ability for the impinging water to freeze on the airframe and other non-rotating components.

(iii) *Liquid water concentration*

This is normally expressed as the number of grams of water per cubic metre of air. The term 'liquid' reflects the supercooled nature of the droplets and also acts to distinguish the state of the cloud from the ice crystal alternative.

In terms of the accretion process, the cloud LWC affects both the type of accretion (rime or glaze) and the rate at which the accretion may form. For large values of LWC, the latent heat which must be removed in order for the impinging droplets to freeze completely is also large, and hence the tendency will be for glaze ice accretion to form. As noted above, as the OAT reduces, increasing the potential to remove latent heat by convective means, the LWC tends also to reduce, and hence the low LWC combined with low OAT will tend to lead to rime ice formation.

Similarly, if during rime ice accretion the LWC is doubled, the rate of ice growth will also be expected to double, assuming rime ice-accretion conditions still exist at the higher LWC. Alternatively, during glaze ice accretion, the total mass of the accreted ice may be expected to increase for a given encounter time, if the LWC is increased.

For helicopter operations with a limited icing clearance capability, which would normally involve flight through stratoform clouds or small cumulus clouds, the average LWC encountered is most likely to be between 0.1 and 0.5 g m^{-3}. However, the JAR-29 and BCAR paper G610 (Gent *et al.* 1996) both specify a larger range of LWC values that must be considered.

In general, the mass of water at the surface of a body will increase linearly with the LWC. Hence the greater the value of the LWC, the greater is the potential for a large accumulation of ice. However, this is not strictly correct, since the collection efficiency of the surface will have an equally important significance in determining the actual mass of water that is incident at the surface. If a large mass of water is contained in droplets of a diameter sufficiently small to have no or little capability to impact on the surface, then the resulting accretion will be small. There is therefore an optimum combination of droplet diameter and LWC which leads to the maximum water impact on the surface for a body of a given size and shape.

(iv) *Volume median diameter (VMD)*

The mass of a water droplet is directly proportional to the cube of its diameter, whereas the influence of the airflow on the droplet is directly proportional to the square of the diameter (neglecting the effect of Reynolds number on the droplet drag coefficient). As a consequence, droplets with large diameter (large mass and hence large inertia) will be less affected by the local aerodynamic forces and will tend to follow a straighter trajectory due to the dominant effect of the inertia forces. In contrast, droplets with small diameter and hence low mass will tend to follow the air streamlines and may not impact on the surface. Hence, whether a droplet impacts the surface or is swept past the body in the airflow depends on the ratio of the inertia to the aerodynamic forces. Put more simply, for a given droplet diameter, large bluff bodies (e.g. a fuselage) at low speed will collect less water than small streamlined bodies travelling at high speed (e.g. a rotor blade).

The diameter of the droplets within any single cloud will vary. The spectrum of droplets that exists in practice is frequently characterized by the VMD of the cloud (sometimes referred to as median volumetric diameter, MVD). This is the diameter above and below which half the mass (or volume) of water is contained.

In general, as the ambient temperature reduces, there will be a tendency for the diameter of the supercooled droplets to reduce, since supercooling is difficult to maintain in large droplets at low temperature. Hence 1 mm diameter supercooled droplets would not be expected to exist at −20 °C. Similarly, for a given cloud, the percentage of the water contained in droplets of diameter above or below the VMD will in general reduce, so that while 40 μm droplets may be present in a cloud which has a VMD of 20 μm, they will nevertheless be relatively few in number. Conversely, droplets with diameter below 10 μm may be numerous, but the mass of water associated with them will be small.

Though this spectrum may vary, historically the Langmuir 'D' distribution (Langmuir & Blodgett 1946) has generally been assumed in analyses to represent the spread likely to be found in practice. A similar distribution of droplets is produced by most spray nozzles in icing wind-tunnels. As a very rough guide, the maximum diameter of the droplets in a cloud is usually of the order of twice the VMD.

The civil FAR-25 and JAR-29 icing envelopes require a range of cloud VMD to be considered. The aircraft manufacturer (or operator) must assess which combination of droplet diameter and water concentration leads to the maximum impact mass of water. The range of diameters (mean effective droplet diameter, which equates to VMD) specified in JAR-29 extends from 15 to 40 μm (50 μm for intermittent icing). This range is considered by the authors to be biased towards the requirements for fixed-wing aircraft. Using the converse to the argument noted above, small droplets (below 15 μm) are unlikely to impact on large chord wings (e.g. 5–7 m root chord on large transport aircraft). Hence it is appropriate for manufacturers of large fixed-wing aircraft to consider the larger droplets contained in a cloud and the large values of the VMD, since the smaller droplets do not contribute significantly to the mass of impacting water, due to the low collection efficiency that results.

However, for a rotor travelling at high subsonic speed, or for the relatively small horizontal stabilizer of a helicopter, the collection efficiency for droplets with diameter 15 μm and lower is likely to remain significant and therefore needs to be addressed. Calculations of the collection efficiency of components based on the VMD of the cloud are thought to be likely to lead to representative estimates of the mass of impinging water. The trajectories of the larger droplets present in clouds should, however, be considered when establishing the limits of water droplet impact on the body, particularly when assessing the chordwise extent required for any ice protection system.

Experience from military icing trials suggests that icing clouds exist with a VMD from as low as 3–4 μm. This is believed to be near to the 'cut-off' diameter, below which no droplet impact will occur on a rotor of chord length *ca.* 0.5 m.

In recent years, the icing hazard posed from clouds with larger droplets has become an important consideration for flight safety. The crash of an ATR-72 aircraft near Roselawn, Indiana in the USA in 1995 with the loss of all on board was attributed to prolonged flight (hold) in freezing drizzle. Freezing drizzle and freezing rain, also termed supercooled large droplets (SLD), form by different process (see § 2 *c* (i)), although in each case the droplet diameter can be considerably larger than for the classical icing case. Freezing drizzle size droplets normally extend from *ca.* 40 to *ca.* 400 μm. Freezing rain droplets are larger still, extending up to several millimetres in diameter. Fortunately, both are associated with relatively warm temperature conditions (−15 to +5 °C, say) and relatively low LWC (*ca.* 0.3 g m^{-3} maximum). However, when encountered by an aircraft, the very high inertia of the droplets leads to near-ballistic trajectories, hardly, if at all, affected by the local flow conditions. Hence the limits of droplet impingement can be extensive and the droplet collection efficiencies will be large in comparison with those for classical icing cloud.

(v) *Airspeed*

This is not in itself an 'icing condition', although it clearly has an effect on the handling and performance of the aircraft. The primary influence in terms of icing severity lies in the fact that the faster the airspeed, the greater the intercepted

volume of air in a given time and hence the greater the mass of water that will be intercepted. It is therefore the product of the collection efficiency, the LWC and the speed of the aircraft/rotor which determines the mass of water that will impact the surface, and hence the amount of accretion.

For rotorcraft, the degrading effects on performance (see § 3), primarily a large increase in profile drag, will be more pronounced at high forward speed, when the excess power available is reduced. Combined with the potential for loss in maximum thrust due to early stall, an unprotected rotorcraft is not expected to be operated in icing conditions at the limiting speed available in clear air. Experience to date suggests that a 10–20 knot reduction in maximum speed over the corresponding clear air values is necessary to allow sufficient margin for flight safety when operating within the envelope of a limited icing clearance.

For fixed-wing aircraft, the reduction in maximum lift that results from ice accretion will lead to an increase in the stall speed and a reduction in the stall angle. As an example, a 35% loss in maximum lift, which is typical of the degradation imposed by ice accretion, would translate to a 24% increase in stall speed, with obvious consequences to safe operation at low speed and landing.

(vi) *Altitude*

As with airspeed, the altitude of the aircraft is not itself directly relevant to the icing severity in terms of the rate of ice accretion. There are, however, a number of important indirect influences of altitude on the icing severity (accretion rate) and the performance and handling of the aircraft and in particular rotorcraft.

The primary influence of altitude on the rate of ice accretion arises from consideration of the likely occurrence of icing conditions in the first instance. Since the air temperature will normally reduce with altitude, the potential for condensation of water droplets and hence icing conditions will increase with height. The study by Roach *et al.* (1984) concludes that, over the UK, the most probable occurrence of icing is in the altitude band of 3000–5000 ft. With other icing parameters (OAT, LWC, VMD, airspeed) held constant therefore, the rate of ice accretion is not expected to be appreciably influenced by the altitude of the aircraft.

Because of the uplift provided in cumulus clouds, the potential for large water concentrations will exist, particularly near the tops of clouds. Also, in stratocumulus layers, because of their dynamics, the LWC will increase with height and the highest LWCs will be found, in general, a few metres from the tops of these layers.

If a rotorcraft is operating close to its maximum thrust capability (maximum thrust coefficient), it is possible for the iced rotor to stall early and, in addition, large power/torque requirements and increased vibration may well limit the capability of the rotorcraft to climb. There have been a number of reports arising from military helicopter operations when the aircraft lost the ability to climb further during flight in icing cloud. Furthermore, on levelling after climbing through cloud, while accreting ice, it has often been found that the power required to maintain level flight was in excess of that allowable. This phenomenon is believed to be a consequence of ice that has accreted on the leading edge of the blade during climbing flight which, on entering level flight, has a greater significance on the drag or lift loss associated with the pitch change and change in the inflow angle of the air through the rotor disc.

For large commercial transport aircraft, the greatly increased operating altitude (typically 30 000–40 000 ft) poses different but important considerations. While the icing conditions may be expected to reduce significantly at very high altitude (tending to encounter ice crystal cloud rather than supercooled water droplets), bleed air available from engines, which is frequently used to anti-ice the wing leading edges, reduces as the altitude increases. A balance is therefore necessary between efficiency of the ice protection systems and the allowable quantity of bleed air that may be used.

3. Effects of icing on aircraft

This section provides a brief description of the likely effects of ice accretion on the performance and handling of aircraft.

(*a*) *Rotorcraft*

The major influences of ice accretion on the handling and performance of rotorcraft are described below and represent an extract of the information available in Gent *et al*. (1996).

The performance of the rotorcraft will be restricted predominantly as a result of ice accretions on the leading edge of rotor blades (assuming unprotected rotors). The ice shapes modify the lift, drag and pitching moment characteristics of the sections. Degradation of the lift characteristics will result in the need for increased collective input to the main rotor, with consequent increased power requirement (torque) for a given flight condition, together with erosion of blade stall margins. Changes to pitching moment characteristics may manifest in increased control loads which may not be obvious to the pilot unless special instrumentation is available. However, by far the most significant effect of ice accretion is likely to be its effect on the profile drag of the section. Large increases in drag, sometimes over very short time periods (e.g. less than 1 min) result in a significant torque rise and care needs to be taken to avoid reaching the limit imposed by either the transmission or the engines. The torque rise may be accompanied by changes in the handling and vibration characteristics of the aircraft.

Margins relative to the rotorcraft blade stall envelope may be eroded such that particular flight conditions in icing may define a revised boundary. It is thus necessary to have an understanding of the baseline rotorcraft blade stall envelope such that some degree of margin may be demonstrated to be maintained.

Structural loads generated within both static and dynamic components require particularly careful consideration for flight in icing conditions. While performance or handling degradation may be quantifiable by aircrew in flight, changes in airframe and component loads are not likely to be directly discernible. Critical components and relevant areas of the airframe are likely to require monitoring and to undergo data gathering activities to ensure that loads remain within acceptable limits and that safe life is consequently not compromised. An instrumented flight test programme is therefore essential before an icing clearance may be granted.

Rotorcraft are particularly and inherently subject to high levels of induced vibration resulting from the rotors and associated transmission systems employed. With high forcing characteristics over a wide range of frequencies, normally acceptable levels of response within the airframe can be compromised by any changes to those forcing influences.

The result of flight in icing conditions can be to change both forcing characteristics and airframe response arising from ice accretions and their associated mass and distribution of mass. Shedding of such accretions from rotors will be almost inevitable owing to the loading environment. Without some form of active de-icing system, shedding is most unlikely to be equally and simultaneously balanced on all blades of any one rotor and may normally be considered asymmetric to some extent. The resultant out of balance of the rotating system may then lead to unacceptable levels of vibration within the airframe.

(*b*) *Fixed-wing aircraft*

This section describes the major influences of ice accretion on the handling and performance of fixed-wing aircraft and represents an extract of the information presented in the AGARD report (1997). General aviation, commuter aircraft and small transport aircraft are more sensitive to the adverse effects of icing than large commercial transport aircraft because of their absolute size. For example, the large C-5A cargo transport aircraft does not have airframe ice protection because the water collection and resulting ice accretion is so low.

As with rotors, ice contamination on wings and tail surfaces reduces maximum lift and stall angle of attack, while increasing profile drag. Ice accretion on propulsion system components like air intakes, engine nacelles, inlet ducts, propellers, fan blades, spinners or inlet guide vanes reduces the propulsion efficiency and adds to aircraft drag.

During take-off, iced aircraft will have an increased ground roll, decreased stall margins and climb rate. Ice on wings and tail surfaces can be particularly hazardous during take-off and can cause serious stability and control problems. In a number of incidents these have led to the loss of the aircraft. During cruise, iced aircraft suffer from a decreased maximum speed capability and efficiency, reduced ceiling height, higher fuel consumption and change in trim characteristics. For smaller aircraft or multi-engined aeroplanes with one or more failed engines, the combination of reduced lift, increased drag and reduced power can result in the loss of the capability to maintain level flight. During approach or landing, the combination of extended flaps and ice on the horizontal tailplane may cause the tailplane to stall, resulting in uncommanded 'pitch-overs' for some aircraft.

Ice on aircraft probes and sensors can lead to inaccurate data such as the wrong airspeed indication or erroneous data supplied to engine control software, leading to incorrect engine power settings and potentially the loss of the aircraft.

Examples of the effect of glaze ice accretion on the lift and drag of an aerofoil are shown in figures 2 and 3, respectively. An example from the AGARD report (1997) suggests that a 35% loss in maximum lift leads to 24% increase in stall speed, which is significant in relation to the 13% margin normally allowed for operations in clear air.

4. Water droplet trajectory calculations

(*a*) *Problem description and assumptions*

The first stage in any icing analysis is to determine where and at what rate the cloud water droplets are deposited on the surface of the body (e.g. wing or fuselage) under investigation. This characteristic is frequently referred to as the water-collection or

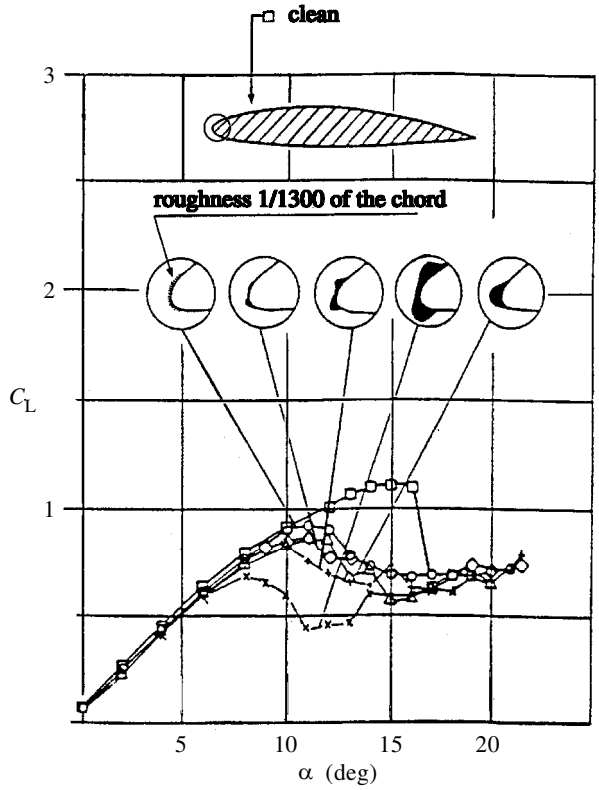

Figure 2. Typical effect of ice accretion on aerofoil lift.

catch-efficiency distribution. The local value of catch efficiency represents the fraction of the freestream water concentration which impacts at a given surface location of the body. The distribution normally has a peak close to the aerodynamic stagnation point and reduces in value to zero at some aft location usually on each of the upper and lower surfaces of the body (aerofoil). Typical peak values range from *ca.* 90% for a rotor with small chord (less than or equal to 0.75 m) and high speed (200 m s^{-1}) to 50% peak or less for large chord wings (greater than or equal to 2 m) at speeds typical of commercial transport aircraft during hold (e.g. 75–140 m s^{-1}).

There are two main types of trajectory calculation in use today. The first and most frequently adopted method is a traditional Lagrangian formulation in which the trajectory of an individual water droplet is tracked from a specified starting point upstream of the body (usually five to seven chord lengths ahead of the body). The second and more recently adopted approach is Eulerian, in which the volume fraction is computed at the same node positions at which the aerodynamic parameters are known. No individual particles are therefore tracked in this approach and the answer leads directly to a measure of the catch efficiency. This approach is particularly useful for complex three-dimensional flow problems and other complex flows such as through rotor and stator blades at the inlet to a jet engine.

For both methods, either a flow solution or a means of calculating the aerodynamic flow is necessary. Methods adopted depend on the application and range from simple panel methods through to full Navier–Stokes solvers.

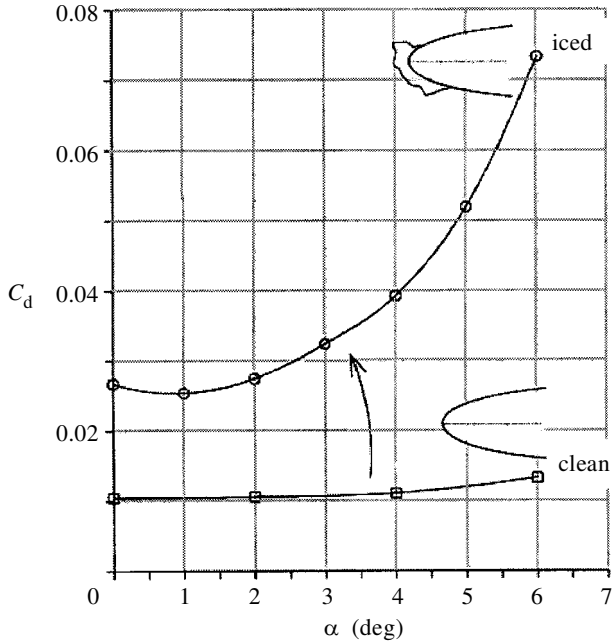

Figure 3. Typical effect of ice accretion on aerofoil drag.

(*b*) *Governing equations*

The derivation of the equation for the droplet acceleration in the x-direction is shown below. The derivation for the acceleration in the y- and z-directions for three dimensional calculations is very similar and therefore not shown. The primary assumptions on which the equations are based are as follows.

(1) The droplets are spherical and do not deform.

(2) There is no collision or coalescence of droplets.

(3) Turbulence effects may be neglected.

(4) The only forces acting on the droplet are due to aerodynamic drag, gravity and buoyancy.

(5) The water droplet concentration is sufficiently small for the droplets to have a negligible effect on the aerodynamic flow and therefore the airflow and water droplets may be treated as independent systems.

An illustration of the coordinate system and terminology employed in this note for the aerofoil and droplet is provided in figures 4 and 5.

In the case of a single particle, where V_a is the local air velocity, u_a is the local air velocity component in the x-direction, v_a is the local air velocity component in the y-direction, V_d is the droplet velocity, u_d is the droplet velocity component in the x-direction, v_d is the droplet velocity component in the y-direction, u_{rel} is the relative air/droplet velocity in the x-direction, v_{rel} is the relative air/droplet velocity

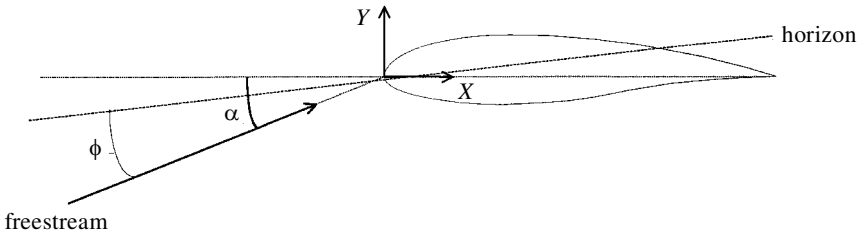

Figure 4. Trajectory coordinate system definition.

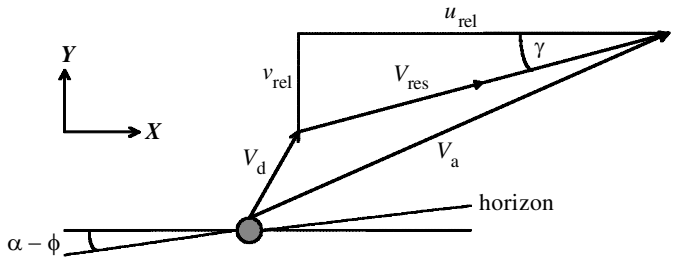

Figure 5. Velocity component definitions.

in the y-direction, V_{res} is the resultant of the relative velocities u_{rel} and v_{rel}, the aerodynamic force on the droplet, F_{a}, is

$$F_{\mathrm{a}} = \tfrac{1}{2} C_{\mathrm{D}} \rho_{\mathrm{a}} A_{\mathrm{d}} V_{\mathrm{res}}^2.$$

The component of this force acting in the x-direction is

$$\begin{aligned} F_{\mathrm{a}x} &= \tfrac{1}{2} C_{\mathrm{D}} \rho_{\mathrm{a}} A_{\mathrm{d}} V_{\mathrm{res}}^2 \cos\gamma \\ &= \tfrac{1}{2} C_{\mathrm{D}} \rho_{\mathrm{a}} A_{\mathrm{d}} V_{\mathrm{res}} u_{\mathrm{rel}}. \end{aligned}$$

Taking u_{d} as the component of the droplet velocity in the x-direction, $F_{\mathrm{a}x}$ as the component of the aerodynamic force in the x-direction, $F_{\mathrm{g}x}$ as the component of the gravitational force in the x-direction, A_{d} as the frontal area of the droplet, D as the droplet diameter, g as the acceleration due to gravity, ρ_{d} as the droplet density (1000 kg m^{-3} for water), ρ_{a} as the air density, m_{d} as the droplet mass, c as the aerofoil chord, C_{D} as the drag coefficient for the droplet, the following expression for the acceleration in the x-direction (in m s^{-1}) may be derived:

$$\frac{\mathrm{d}u_{\mathrm{d}}}{\mathrm{d}t} = \frac{F_{\mathrm{a}x} + F_{\mathrm{g}x}}{m_{\mathrm{d}}}.$$

Using the following expressions,

$$\begin{aligned} m_{\mathrm{d}} &= \rho_{\mathrm{d}} \times \tfrac{4}{3}\pi\tfrac{1}{8} D^3, \\ A_{\mathrm{d}} &= \tfrac{1}{4}\pi D^2, \\ F_{\mathrm{g}x} &= m_{\mathrm{d}} g \left(1 - \frac{\rho_{\mathrm{a}}}{\rho_{\mathrm{d}}}\right) \sin(\alpha - \phi), \\ \frac{\mathrm{d}u_{\mathrm{d}}}{\mathrm{d}t} &= \frac{\tfrac{1}{2} C_{\mathrm{d}} \rho_{\mathrm{a}} \pi \tfrac{1}{4} D^2 V_{\mathrm{res}} u_{\mathrm{rel}}}{\tfrac{4}{24} \rho_{\mathrm{d}} \pi D^3} + \frac{m_{\mathrm{d}} g}{m_{\mathrm{d}}} \left(1 - \frac{\rho_{\mathrm{a}}}{\rho_{\mathrm{d}}}\right) \sin(\alpha - \phi), \end{aligned}$$

we have

$$\frac{\mathrm{d}u_\mathrm{d}}{\mathrm{d}t} = \frac{18C_\mathrm{d}\rho_\mathrm{a}V_\mathrm{res}u_\mathrm{rel}}{24\rho_\mathrm{d}D} + \left(1 - \frac{\rho_\mathrm{a}}{\rho_\mathrm{d}}\right)g\sin(\alpha - \phi).$$

This can be further simplified by making a substitution using the droplet Reynolds number,

$$R = \frac{\rho_\mathrm{a}V_\mathrm{res}D}{\mu},$$

yielding

$$\frac{\mathrm{d}u_\mathrm{d}}{\mathrm{d}t} = \frac{18C_\mathrm{d}R\mu u_\mathrm{rel}}{24\rho_\mathrm{d}D^2} + \left(1 - \frac{\rho_\mathrm{a}}{\rho_\mathrm{d}}\right)g\sin(\alpha - \phi).$$

This can be written in non-dimensional form using the non-dimensional terms

$$\bar{u}_\mathrm{d} = \frac{u_\mathrm{d}}{V_\infty}, \qquad \bar{t} = \frac{tV_\infty}{c}, \qquad \bar{u}_\mathrm{rel} = \frac{u_\mathrm{rel}}{V_\infty},$$

$$\frac{\mathrm{d}\bar{u}_\mathrm{d}}{\mathrm{d}\bar{t}} \times \frac{V_\infty^2}{c} = \frac{18C_\mathrm{d}R\mu\bar{u}_\mathrm{rel}V_\infty}{24\rho_\mathrm{d}D^2} + \left(1 - \frac{\rho_\mathrm{a}}{\rho_\mathrm{d}}\right)g\sin(\alpha - \phi),$$

so that

$$\frac{\mathrm{d}\bar{u}_\mathrm{d}}{\mathrm{d}\bar{t}} = \frac{18C_\mathrm{d}R\mu c\bar{u}_\mathrm{rel}}{24\rho_\mathrm{d}D^2V_\infty} + \left(1 - \frac{\rho_\mathrm{a}}{\rho_\mathrm{d}}\right)\frac{c}{V_\infty^2}g\sin(\alpha - \phi).$$

Similarly,

$$\frac{\mathrm{d}\bar{v}_\mathrm{d}}{\mathrm{d}\bar{t}} = \frac{18C_\mathrm{d}R\mu c\bar{v}_\mathrm{rel}}{24\rho_\mathrm{d}D^2V_\infty} - \left(1 - \frac{\rho_\mathrm{a}}{\rho_\mathrm{d}}\right)\frac{c}{V_\infty^2}g\cos(\alpha - \phi).$$

Furthermore, introducing the inertia parameter

$$K = \frac{\rho_\mathrm{d}D^2V_\infty}{18\mu c},$$

we have

$$\frac{\mathrm{d}\bar{u}_\mathrm{d}}{\mathrm{d}\bar{t}} = \frac{C_\mathrm{d}R\bar{u}_\mathrm{rel}}{24K} + \left(1 - \frac{\rho_\mathrm{a}}{\rho_\mathrm{d}}\right)\frac{c}{V_\infty^2}g\sin(\alpha - \phi)$$

and

$$\frac{\mathrm{d}\bar{v}_\mathrm{d}}{\mathrm{d}\bar{t}} = \frac{C_\mathrm{d}R\bar{v}_\mathrm{rel}}{24K} - \left(1 - \frac{\rho_\mathrm{a}}{\rho_\mathrm{d}}\right)\frac{c}{V_\infty^2}g\cos(\alpha - \phi).$$

The equations of motion are readily solved using Runge–Kutta or similar numerical methods, with the initial droplet velocity at the trajectory starting point several chord lengths ahead of the body usually assumed to be the same as that of the aerodynamic flow.

(*c*) *Flow solution*

In order to evaluate the trajectory of a droplet, the air velocity must be known or calculable at every position the droplet occupies. In practice, aircraft icing engineers will normally employ codes already developed to model the flow around the

component of interest, whether this be for internal flows such as in engine intakes, or external flows.

For ease of operation, the majority of two-dimensional ice-accretion codes have a flow solver embedded within the trajectory code. In the case of LEWICE (Wright 1995) and TRAJICE2 (Gent 1994*b*), these are inviscid incompressible-flow panel methods. Somewhat surprisingly, the use of relatively basic methods has been found not to affect results significantly. The use and added complexity of more refined methods is not therefore justified for many applications, at least up to Mach numbers of *ca.* 0.4. With panel methods, the flow solution is evaluated at each position of the droplet trajectory by summing the contribution to the flow from the calculated circulation from a series of panels that describe the aerofoil or body profile. The flow solution at the surface of the profile is also required in the accretion analysis. The alternative is a grid-based solution in which the velocity is known at discrete node points of a grid around the body. The velocity at a given point in space is then estimated by interpolation using the surrounding grid nodes. The code described in Gent (1984) employed a grid-based solution written around an existing transonic flow solver.

For three-dimensional flow cases, the options remain the same, either embedding a flow solver in the trajectory code or using a flow solution obtained for a grid of points surrounding the body under investigation. The ICECREMO three-dimensional icing code has been developed to accept any structured grid flow solution (see Bartlett 2000). This maximizes the range of the potential applications of the code, since existing solvers for internal flows (engine intakes), external (wings) or rotating flows (rotors) can be analysed without the need for further development.

(*d*) *Droplet drag law*

The basis for most droplet trajectory calculations for the classical icing cloud (droplet VMD *ca.* 20 μm) is that the droplets remain spherical due to their small size and hence dominant surface tension force. Accordingly, the drag law employed by Gent (1984) has been found to give good results. This drag law is expressed as

$$\tfrac{1}{24}C_{\mathrm{D}}R = 1 + 0.197R^{0.63} + 2.6 \times 10^{-4}R^{1.38}.$$

However, with the recent focus on SLD cloud and the corresponding significantly larger droplet size, the validity of the above assumption is called into question. A better approximation for the drag coefficient for larger droplets when their shape becomes flattened and no longer spherical is available in Hansman (1984). This drag law states that, for $R > 3500$,

$$\tfrac{1}{24}C_{\mathrm{D}}R = (1.699 \times 10^{-5})R^{1.92}.$$

In practice, for very large droplets, the inertia forces are found to be so dominant in relation to the aerodynamic forces that the precise drag law has little effect on the calculated trajectories, which tend to be ballistic (i.e. straight lines) in nature.

Finally, it is perhaps worth noting that in the case of SLD cloud, the assumption that the droplet is initially travelling at the same speed as the local air velocity is no longer valid. The terminal velocity of a droplet may be calculated using the following expression, obtained by equating the gravitational force and the aerodynamic drag

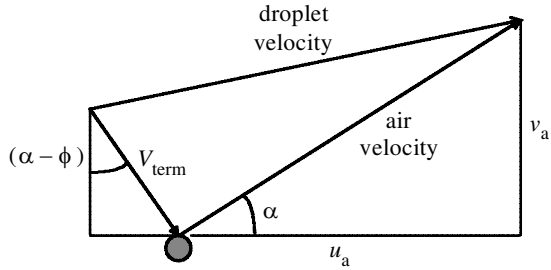

Figure 6. Determination of initial droplet velocity.

experienced at the terminal velocity,

$$V_{\text{term}} = \sqrt{\frac{4Dg(\rho_{\text{d}} - \rho_{\text{a}})}{3\rho_{\text{a}} C_{\text{D}}}},$$

where D is the droplet diameter, g is the acceleration due to gravity, ρ_{d} is the droplet density, ρ_{a} is the air density, C_{D} is the drag coefficient for the droplet.

It can be seen that the terminal velocity of the droplet is a function of its drag coefficient. Since the drag coefficient is a function of the droplet Reynolds number, which is proportional to V_{term}, an iterative process is required to find V_{term}. The accuracy of this formula was tested by comparing the predicted terminal velocity of different sized droplets with those determined by experiment (see Mason 1971). A good correlation was found between predicted and experimental results.

The initial droplet velocity components (dimensionless) can now be calculated by resolving the air velocity and the terminal velocity (as illustrated in figure 6),

$$u_{\text{d}} = u_{\text{a}} + \frac{V_{\text{term}}}{V_\infty} \sin(\alpha - \phi),$$

$$v_{\text{d}} = v_{\text{a}} - \frac{V_{\text{term}}}{V_\infty} \cos(\alpha - \phi),$$

where u_{d} is the droplet velocity component in the x-direction, v_{d} is the droplet velocity component in the y-direction, (dimensionless with respect to V_∞), u_{a} is the air velocity component in the x-direction, v_{a} is the air velocity component in the y-direction, V_{term} is the terminal velocity of the droplet relative to the air velocity (m s^{-1}) and α, ϕ are angles as defined in figures 4 and 6 above.

(*e*) *Collection efficiency*

The preceding subsections have shown how the trajectory of a water droplet may be calculated in the case of an aircraft wing. From these calculations, the start (user-specified) and impact (calculated) positions of the droplet are available. A number of schemes are available for the calculation of collection efficiency from predetermined particle tracks. All methods relate initial cross-sectional area of the droplet stream tube to the area at impact on the surface. For the method described by Gent (1984), where two-dimensional flow conditions are modelled, the method evaluates two additional trajectories, each a small displacement either side of the original trajectory. The local value of the collection efficiency, β, is then approximated using the definition illustrated in figure 7, where δy is the total separation between trajectories in

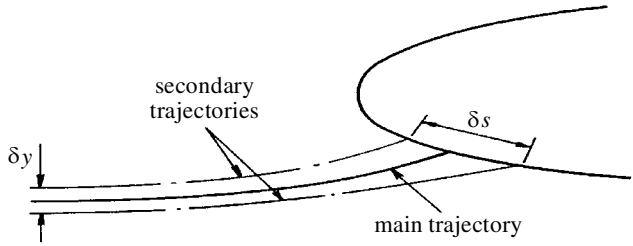

Figure 7. Method used to calculate local catch efficiency, $\beta = \delta y/\delta s$.

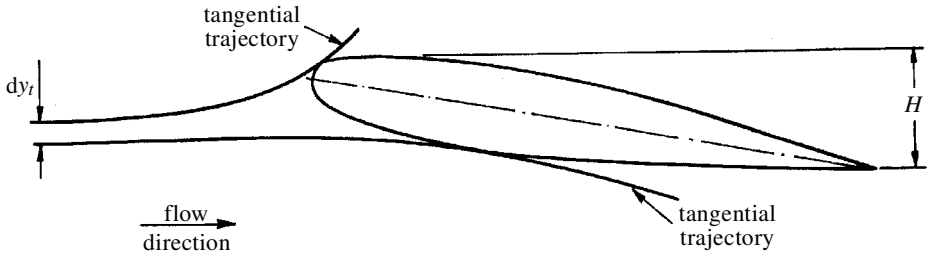

Figure 8. Definition of the overall catch efficiency, $E = \mathrm{d}y_t/H$.

the freestream and δs is the total separation between the trajectories at impact on the surface.

However, in the AGARD report (1997), the collection efficiency is obtained directly from the slope of the curve fitted through a set of initial and impact point trajectory data, namely,

$$y_0 = f(s), \qquad \beta = \frac{\partial y_0}{\partial s}.$$

An alternative parameter sometimes used in icing analysis is the overall catch efficiency, E, defined as illustrated in figure 8. This parameter represents a measure of the total water collection of the body.

In three-dimensional flow situations, the area ratio (see figure 9) is frequently employed using several (more than two) trajectories, but is sometimes estimated from the normal product of an individual trajectory at impact.

(*f*) *Review of existing codes*

Codes for trajectory calculations suitable for computation of two-dimensional flow cases have been developed and validated by Wright (1995), Guffond & Brunet (1985), Gent (1984, 1994*b*) and, more recently, by Habashi *et al.* (1998*b*) and Mingione *et al.* (1999). Codes have also previously been developed by Lozowski & Oleskiw (1983) and Meijer (1987).

Corresponding codes for three-dimensional flow cases are less widely used within industry at this time, although codes for external flow have been developed by Bidwell & Potapczuk (1993), Caruso (1994), Hedde & Guffond (1993) and Dart (1995).

Codes suitable for analysing axisymmetric bodies such as spinners have been developed by Gent (1994*c*) and, for engine nacelles, by Kim (1986). Codes suitable for the analysis of droplet trajectories within engines have been developed by

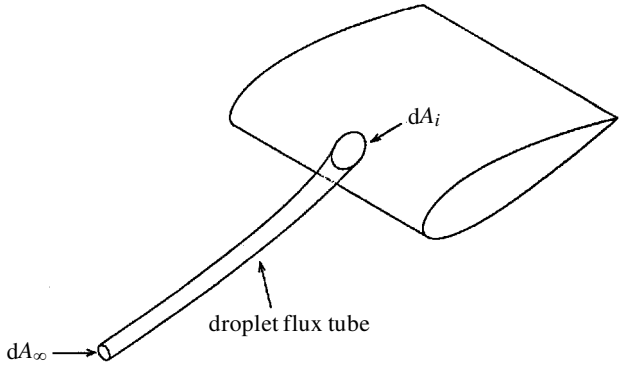

Figure 9. Definition of the local catch efficiency on a three-dimensional geometry, $\beta = dA_\infty/dA_i$.

Tan (1991) for Rolls-Royce plc (UK), who, in turn, have developed an advanced code (T. R. Kingston 1996, unpublished work).

(*g*) *Example results*

In view of the potentially vast number of cases that could be analysed, this section provides only a brief selection of data, sufficient to give the reader a broad understanding of the important parameters.

(i) *Parametric results*

By way of example, the DERA code TRAJICE2 has been run to illustrate the effects of key parameters on the collection efficiency distribution. Additional results are presented by Gent (1984, 1994*b*), while a comparison of results against other droplet trajectory codes may be found in Bidwell & Mohler (1995). The results in figure 10 show the effect of aerofoil chord, droplet size, airspeed, temperature and altitude on the amount of water intercepted for conditions similar to the wing of a turboprop aircraft. The wing incidence was taken to be 4°.

It will be seen that aerofoil chord and droplet size have a marked effect on water catch, whereas airspeed, once above a certain threshold, altitude and temperature have a much smaller effect.

(ii) *Accuracy checks*

Examples of the accuracy that may be achieved from a two-dimensional trajectory analysis code may be found in Gent (1994*b*) and Gent *et al.* (1993). An example of a relatively close agreement is shown in figure 11. This shows a comparison between predicted results obtained by Gent (1994*b*) and results measured by NASA from experimental tests conducted in the 1950s. The results show that a single calculation based on the VMD is likely to provide a reasonably accurate indication of the total mass of water impacting on the surface. However, accurate estimates for the limits of droplet impingement require the actual spectrum of droplets to be analysed.

Examples of the accuracy of a three-dimensional calculation may be found in Dart (1995) and particularly in Bidwell & Mohler (1995), which shows an extensive

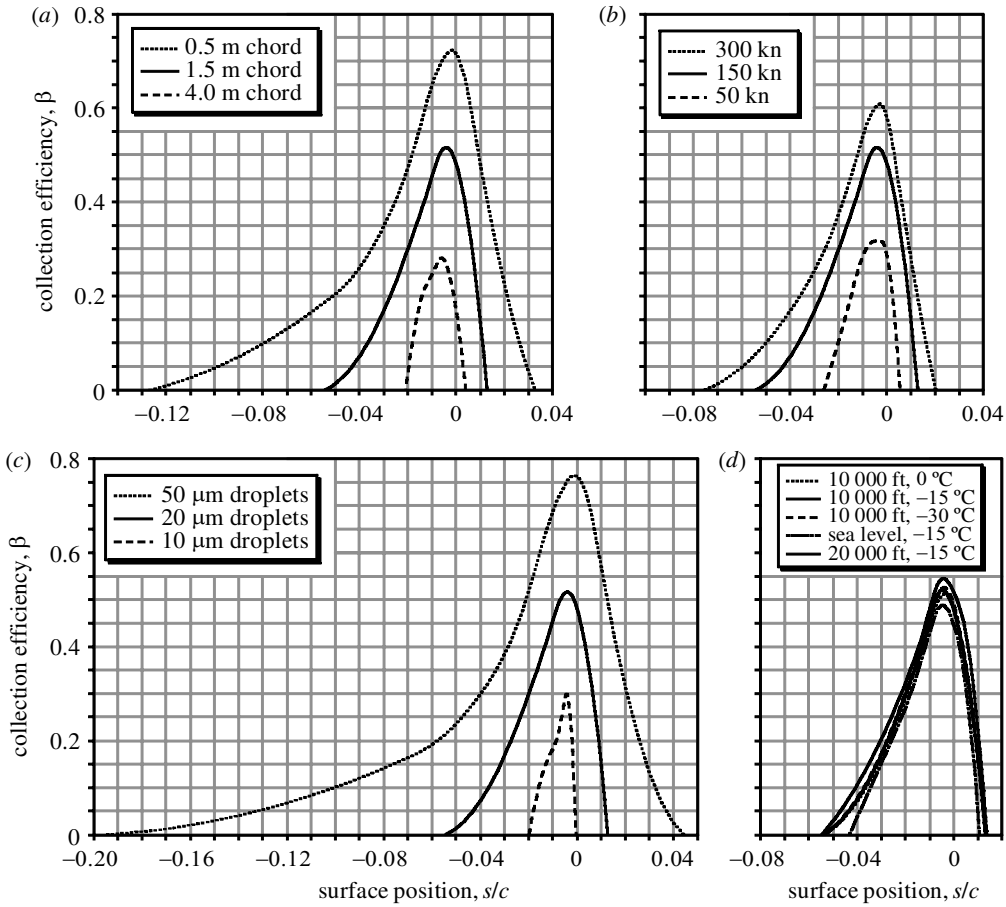

Figure 10. Illustration of the effect of the key parameters ((*a*) aerofoil chord, (*b*) airspeed, (*c*) droplet diameter, (*d*) altitude and OAT) on water collection efficiency.

range of comparisons for the NASA three-dimensional code. An example of a three-dimensional catch is shown in figure 12, which is taken from Dart (1995). This is a comparison against the experimental data reported in Bidwell & Mohler (1995) for a 30° swept NACA 0012 section wing.

(*h*) *Limitations and future research required*

The codes available for steady two-dimensional flow appear to be well validated against experimental data, although care still needs to be exercised when applying them. For instance, a calculation based on VMD only is unlikely to give an accurate indication of the limits of droplet impingement which are determined by the larger droplets contained within the cloud spectrum. Accurate impact limit calculations therefore require knowledge of the droplet spectrum. Also, for large chord wings and bodies, it may again provide inaccurate results if droplet trajectory calculations are based on VMD rather than individual droplet sizes. Fortunately, the civil certification requirements prescribe the droplet diameter range to be investigated.

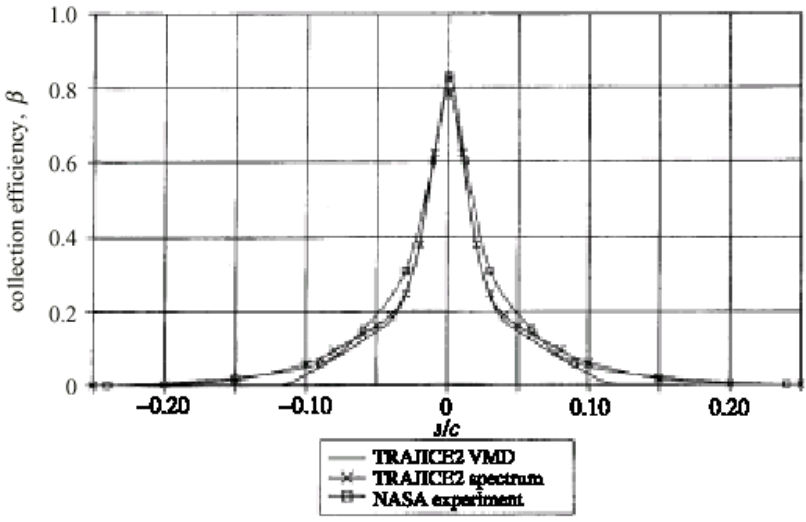

Figure 11. Comparison between predicted collection efficiencies and experimental results on a NACA 0012 aerofoil. TRAJICE2 spectrum: from Ministry of Defence standard 00-970, vol. 1, ch. 712/2. Incidence is 0°, airspeed is 81 m s^{-1}, VMD is 20.4 μm, temperature is 7.3 °C, pressure is 94.54 kPa.

The level of validation of three-dimensional codes is less well established and further work is required in this area. Experimental data tend to be proprietary and not published widely, although a source is given Bidwell & Mohler (1995). Individual validation results may be found in the references to the codes cited in § 4 *f*.

Very little work has been done to validate trajectories in unsteady flows such as exist on a rotor or in gas turbines, although both cases can now be analysed. In the case of rotors, Gent *et al*. (1987) treated a rotor as a pseudo-unsteady problem by assuming instantaneous water catch was proportional to instantaneous speed and incidence. The data were then averaged over the rotor azimuth. Rolls-Royce similarly have a capability to model particles, including water droplets, through the various inlet stages of a gas turbine.

5. Ice-accretion prediction

(*a*) *Problem description and assumptions*

Having determined, using droplet-trajectory analysis, where and at what rate the cloud droplets impact on the surface it is now necessary to determine how the water will freeze to form an ice accretion. In order for the supercooled water droplets to freeze, they must release their latent heat. This is achieved by a combination of heat conduction into the body on which the droplets have impacted and by heat exchange with the air, primarily through evaporative and convective heat transfer processes.

The classical approach to ice-accretion prediction is that of Messinger (1953), which assumes that the icing of a surface is governed by the balance of a number of heat flows, e.g. kinetic heating, convective cooling, evaporative cooling, latent heat of freezing and a number of sensible heat terms. These terms are described more fully

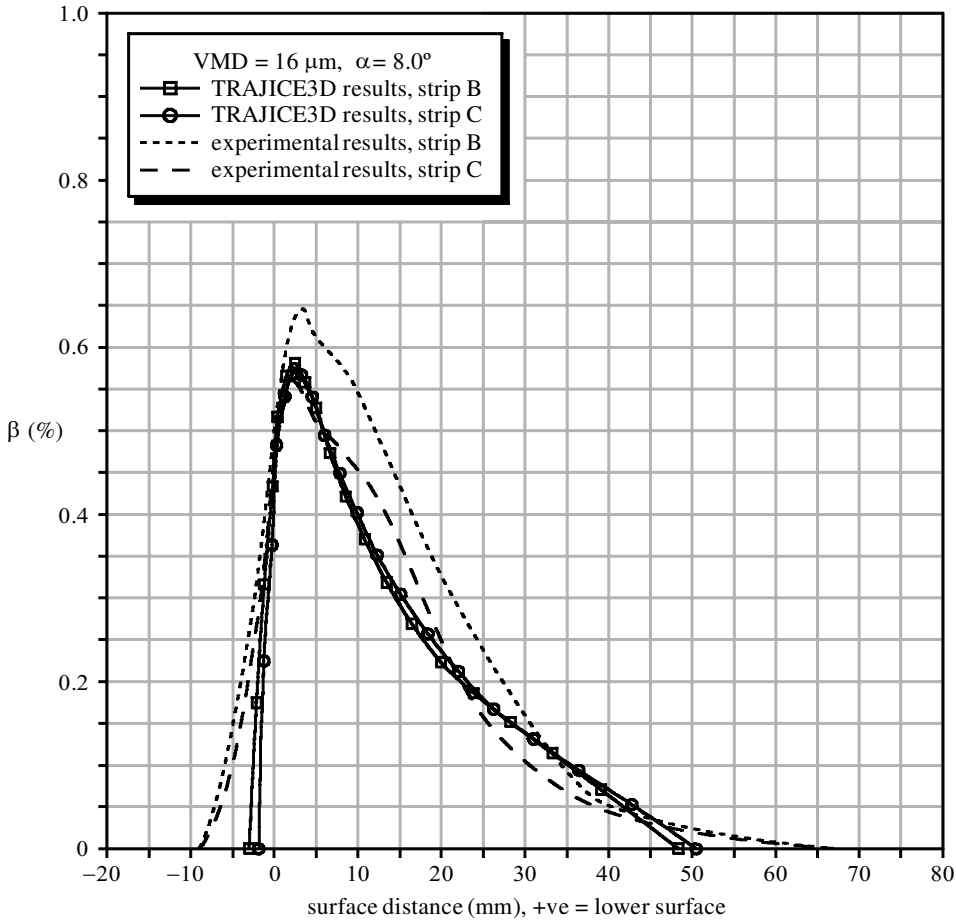

Figure 12. Example of the accuracy of a 3D catch efficiency calculation on a swept wing.

in § 5 *b*. It is therefore an energy balance, which in practice is evaluated at a series of discrete positions around the leading edge of the body under investigation. With this 'control volume' approach, the calculation normally commences at the airflow stagnation point. The surface temperature and a parameter known as the freezing fraction, N_f, are evaluated. The latter represents the proportion of the incident water which freezes at a specified location. Any unfrozen water is assumed to flow back, termed 'runback water', along the surface and is included in the analysis of the next downstream control volume.

From the freezing fraction, the rate of ice growth may be estimated and the ice profile predicted by suitable extrapolation of the growth rates to a given finite time in icing. Depending upon the code, the calculations may be repeated for the new airflow, water catch and ice accretion on the ice-deformed surface.

The Messinger approach is the foundation of most of the ice-accretion prediction codes in use today. The method was updated by Cansdale & Gent (1983) to allow for air compressibility effects, but has changed little otherwise. When solving the heat balance equations, many researchers adopt the simpler adiabatic surface assump-

tion. Without heat conduction within the structure or the ice, the equations are not coupled and may be solved by direct substitution, as indicated above.

For rotorcraft, Gent *et al.* (1987) showed that heat conduction within practical rotor blade constructions was small and the adiabatic surface approximation is therefore satisfactory for accretion on unheated rotors. However, for accretion on bodies with good thermal conductivity and/or high thermal mass, the heat conduction within the structure and any accreted ice may need to be considered. The leading edge of the wings on commercial passenger aircraft are frequently manufactured from a lightweight alloy in the shape of a hollow 'D' spar, the material of which is a good conductor, although the thickness of the material is usually relatively small (less than a few millimetres) and therefore heat conduction is again considered unlikely to be significant.

However, in the past, some scale wind-tunnel models have been manufactured for convenience out of solid aluminium and have had a relatively large metallic mass close to the leading edge. Such test specimens may therefore be expected to accrete ice slightly differently in icing-tunnel tests than models constructed from insulating material, due to the differences in the heat conduction within the model. The thermal mass of the body can also affect the initial period of ice accretion (much less than 1 min), with heat stored in the body potentially enhancing or delaying accretion on the surface depending upon the total temperature (negative or positive total temperature, respectively) of the local surface. In the case of enhanced cooling, the ice type may also change from, say, rime to glaze ice over a very short period of time during the initial exposure to icing cloud. If present, this phenomenon is easily discernible if the crystal structure of the ice is analysed. Hammond (1998) observed for some ice accretions that the grain structure of the ice was noticeably smaller during the initial periods of accretion, with fine grain size associated with rime type accretion closely followed by a coarse grain size, which is associated with glaze ice accretions, subsequently forming at the accretion surface.

If additional heat is to be provided to the surface, such as from an ice-protection system, then ice-accretion modelling similarly needs to include the effects of transient heat flows to and from the ice and therefore a transient icing analysis is appropriate. For the modelling of electrothermal rotor de-icing systems, Gent (1995) has incorporated a transient icing analysis which allows for heat conduction within a multi-layered structure. More recently, Myers & Hammond (1999) have developed a general transient ice-accretion prediction as part of the ICECREMO project. This project is associated with the development of a general ice-accretion prediction code suitable for application to bodies in three-dimensional flows.

(*b*) *Governing equations*

The classic Messinger approach for incompressible flows assumes that the icing of a surface is governed by balance of a number of heat flows. These include air kinetic heating (Q_{ke}), water droplet impact heating (Q_{kew}), convective cooling (Q_{c}), evaporative cooling (Q_{e}), latent heat of freezing (Q_{Le}), sensible heat from the impinging water (Q_{sw}) droplets and sensible cooling of the ice mass (Q_{si}), where appropriate, and sensible heat from any runback water (Q_{srbw}).

Cansdale & Gent (1983) extended the analysis to compressible flow by introducing the following changes.

(a) Combining the convective cooling and air kinetic heating terms.

(b) Adding a new evaporative cooling term which allows for the effect of pressure distribution around the aerofoil on the local water vapour concentration.

Hence

$$Q_{\mathrm{c}} - Q_{\mathrm{ke}} = h_{\mathrm{c}}(t_{\mathrm{s}} - t_{\mathrm{r}}),$$

where h_{c} is the convective heat transfer coefficient, t_{s} is the surface temperature and t_{r} is the dry adiabatic recovery temperature. The recovery temperature is evaluated from the following equation:

$$t_{\mathrm{r}} = \left(t_\infty + 273.15 + \frac{V_\infty^2}{2C_p}\right)\left(\frac{1 + r(\frac{1}{5}M_{\mathrm{L}}^2)}{1 + \frac{1}{5}M_{\mathrm{L}}^2}\right) - 273.15,$$

where t is the temperature, V is airspeed, C_p is the air specific heat capacity, M is the Mach number and r is the recovery factor (equal to $Pr^{0.33}$ for turbulent flow). The subscripts ∞ and L indicate freestream and local, respectively.

The new expression for evaporative cooling, explained in Cansdale & Gent (1983), is

$$Q_{\mathrm{e}} = \frac{0.622 h_{\mathrm{c}} L_{\mathrm{v}}}{C_p H_0 Le^{2/3}}\left(e_{\mathrm{s}}\left(\frac{T_{\mathrm{T}}}{T_{\mathrm{s}}}\right)\left(\frac{P_{\mathrm{L}}}{H_0}\right)^{-1/\gamma} - e_\infty\left(\frac{H_0}{P_\infty}\right)\right),$$

where L_{v} is the latent heat of vaporization, P is static pressure, H_0 is total pressure, T_{T} is the total temperature in kelvin, e is the water vapour pressure and Le is the Lewis number. Subscripts are as above, with s indicating properties at the surface.

The freezing fraction N_{f} within a small control volume may thus be evaluated from

$$Q_{\mathrm{c}} - Q_{\mathrm{ke}} + Q_{\mathrm{e}} + Q_{\mathrm{sw}} = Q_{\mathrm{L}} + Q_{\mathrm{kew}} + Q_{\mathrm{srbw}},$$

with (noting that $t_{\mathrm{f}} = 0$ and M_{w} is the mass water catch rate)

$$\begin{aligned} Q_{\mathrm{sw}} &= M_{\mathrm{w}} C_{p\mathrm{w}}(t_{\mathrm{f}} - t_\infty), \\ Q_{\mathrm{L}} &= N_{\mathrm{f}}(1 + X) M_{\mathrm{w}} L_{\mathrm{F}}, \\ Q_{\mathrm{kew}} &= 0.5 M_{\mathrm{w}} V_{\mathrm{i}}^2, \\ Q_{\mathrm{srbw}} &= X M_{\mathrm{w}} C_{p\mathrm{w}}(t_{\mathrm{rbw}} - t_{\mathrm{s}}), \end{aligned}$$

in which the impact speed V_{i} is frequently approximated to the freestream speed V, and X is the runback rate expressed as a fraction of the directly impinging water mass catch rate. Substituting the above and rearranging gives

$$N_{\mathrm{f}} = \lambda\vartheta\left(e_{t_{\mathrm{ft}}}\left(\frac{T_{\mathrm{T}}}{273.15}\right)\beta^{1/\gamma} - e_{t_\infty}\chi\right) - \lambda\left(t_{\mathrm{r}} + b\left(\frac{V_\infty^2}{2C_{p\mathrm{w}}} + t_\infty + X t_{\mathrm{rbw}}\right)\right),$$

where

$$\lambda = \frac{C_{p\mathrm{w}}}{bL_{\mathrm{f}}(1 + X)}, \qquad b = \frac{M_{\mathrm{w}} C_{p\mathrm{w}}}{h_{\mathrm{c}}}, \qquad \vartheta = \frac{0.622 L_{\mathrm{v}}}{C_p H_0 Le^{2/3}}$$

and γ is the air specific heat ratio (1.5).

In most codes, the above expression is evaluated and additional calculations are then performed using the following criteria.

(i) $N_f > 1.0$, reset $N_f = 1$ and solve for $t_s < 0$.

(ii) $N_f < 0$, reset $N_f = 0$ and solve for $t_s > 0$.

No further calculations are required if $0 \leqslant n_f \leqslant 1$, since the solution is $t_s = 0$. Note that for $t_s < 0$, the additional term $Q_{sc} = N_f M_w C_{pi}(t_f - t_s)$ is required. The heat exchange expressions above can be rearranged to give t_s when $t_s \neq 0$.

(*c*) *Convective heat transfer coefficient*

By far the most important and, in turn, difficult parameter essential for accurate prediction of glaze ice accretion is the convective heat transfer coefficient. Though information from computational fluid dynamic (CFD) codes may be available, this is at best likely to be appropriate to the clean surface, and therefore of no use. Most analyses do not include the effects of either surface roughness or the profile change caused by the ice. Gent (1994*b*) produced an empirical analysis using scaling of experimental results from the heat transfer of a roughened cylinder reported by Achenbach (1977). The leading edge of the aerofoil is approximated by an equivalent cylinder. This provided an early breakthrough in glaze ice-accretion prediction, but is really only valid for small accretions (usually less than 2% chord in thickness) and is only appropriate to the initial prediction (i.e. first step) of the ice on the clean aerofoil and cannot be used on subsequent steps because the cylinder profile assumption is no longer valid.

Both NASA and ONERA employ an integral boundary layer method in their ice-accretion prediction codes. DERA also use this method for its code as an alternative, and it has also been used more recently by other researchers. With this technique, details of the laminar and turbulent boundary layers are calculated with transition determined via a roughness Reynolds number. The effects of roughness are included by evaluating parameters at the roughness height, which is defined in terms of an equivalent sand grain roughness. For laminar flow, the equation of Smith & Spalding (1958) is adopted to calculate the convective heat transfer coefficient,

$$h_c = \frac{0.296k}{\sqrt{\mu/\rho}} \sqrt{V^{2.87} \Big/ \int_0^s V^{1.87}\,\mathrm{d}s},$$

where k is the thermal conductivity of air, s is the surface distance from the stagnation point, μ is the dynamic viscosity of air, ρ is the air density and V is the velocity at edge of boundary layer.

The derivation was made assuming that the Prandtl number for air is constant at 0.7 and the surface has a constant temperature. These approximations are considered to be adequate for the accuracy required.

Note that the equation above for laminar heat transfer coefficient is not dependent on roughness. For turbulent flow, the method from Kays & Crawford (1980) is adopted. If the classical method is being used *or* if there is a favourable pressure gradient, the formulae below can be used. The turbulent momentum thickness, δ_2, is obtained from

$$\delta_2 = \frac{0.036(\mu/\rho)^{0.2}}{V^{3.29}} \left(\int_{s_{trans}}^{s} V^{3.86}\,\mathrm{d}s \right)^{0.8} + \delta_{2,trans},$$

where $\delta_{2,\mathrm{trans}}$ is the laminar momentum thickness at transition. The skin friction coefficient may then be obtained from

$$\tfrac{1}{2}c_\mathrm{f} = \frac{0.168}{[\ln(864\delta_2/k_\mathrm{s} + 2.568)]^2},$$

which allows the Stanton number to be calculated from

$$St = \frac{\frac{1}{2}c_\mathrm{f}}{Pr_\mathrm{t} + \sqrt{\frac{1}{2}c_\mathrm{f}}/St_k},$$

where $Pr_\mathrm{t} = 0.9$ for the turbulent boundary layer.

The roughness Stanton number is calculated using the equation

$$St_k = 1.92Re_k^{-0.45}Pr^{-0.8},$$

where Re_k is the roughness Reynolds number defined as

$$Re_k = \frac{\rho V k_\mathrm{s}}{\mu}.$$

The turbulent convective heat transfer coefficient can then be evaluated using the formula

$$h_\mathrm{c} = St\rho V c_p,$$

where c_p is the specific heat capacity at constant pressure for air.

Transition from laminar to turbulent flow is assumed to occur on the iced surface when the roughness Reynolds number exceeds a critical value (typically $Re_k \geqslant 600$).

Note that a value for the surface roughness must be input to the above equations. This can either be user defined or estimated within the code. For instance, early versions of the LEWICE code used an empirical correlation based on freestream velocity, LWC and surface static temperature. A similar expression is used in TRAJICE2. The ONERA code uses a fixed non-dimensionalized roughness height of $0.001x/c$. However, more recent versions of LEWICE (Wright *et al*. 1997) are stated to use the following expression which attempts to include more of the physics,

$$k = \left(\frac{4\sigma\mu^2}{\rho F\tau}\right)^{1/3},$$

where σ is the surface tension, μ is the viscosity of water, ρ is the water density, τ is the surface shear stress and F is the fraction of the surface that is wetted.

The above methods have been shown to work reasonably well in the two-dimensional flow cases. It should be noted that in most implementations the analysis is applied in a single iteration, using local flow velocity obtained from the inviscid solutions usually available to the icing calculations. This is a very crude approximation and more rigorous calculation of the boundary layer parameters is highly desirable since, at present, the effect of the boundary layer on the flow is neglected.

To date, little appears to have been done to calculate the heat transfer coefficient for three-dimensional flows. As far as is known, all researchers adopt the two-dimensional approach above, having used aerodynamic analysis to identify streamlines on the body to use for the integral boundary-layer analysis. This itself may be a

complex task since the airflow direction at the surface may be different to the direction of the flow at the edge of the boundary layer, owing to the three-dimensional effects. Hence the flow direction at the edge of the boundary layer is not sufficient to determine the streamlines on the surface. Furthermore, if centrifugal effects are present for rotating components, the water runback direction may not be in the same direction as the airflow at the surface.

(*d*) *Review of existing codes*

The well-established codes were reviewed briefly in § 5 *a* and cover the three major research centres of ONERA, NASA and DERA. Codes referenced in § 4 *f* for droplet trajectory calculations are also appropriate for ice-accretion prediction since few codes stop at the trajectory analysis stage. The reader should therefore consult § 4 *f* for additional references.

(*e*) *Example results*

(i) *Parametric results*

By way of example, the DERA code TRAJICE2 has been run to illustrate the effects of key parameters on the ice profile. Additional results are presented in Caruso (1994), Cebeci (1989) and Dart & O'Brien (1996), while a comparison of results against other ice-accretion prediction codes may be found in Wright *et al.* (1997). The results in figure 13 show the effect of LWC, OAT, airspeed, chord and droplet size on the ice profile. The physical dimensions and aerodynamic conditions chosen for the baseline case are similar to those that could be experienced by the main wing of a small turboprop aircraft.

(ii) *Accuracy checks*

The main conclusion from Wright *et al.* (1997) is that the three codes developed by NASA, ONERA and DERA were basically equivalent in terms of their accuracy. Though results from one particular code may be more accurate than the other two in certain cases, overall, the codes provided a similar level of accuracy. It is therefore difficult to give a precise impression of the accuracy of the codes here, since examples over a wide range of conditions are required. The reader is referred to the various references provided in this report if more detailed information is required concerning code accuracy. For the purposes of illustration, one good (figure 14*b*), one fair (figure 14*c*) and one poor (figure 14*a*) comparison between measurement and theory are shown. It should be noted that until very recently there was no measure of the discrepancy between theoretical and measured results, which was purely subjective. The work of Ruff (1999) should enable a more quantitative estimate of accuracy to be made in the future.

(*f*) *Limitations and future research required*

The accuracy and limitations of ice-accretion codes for two-dimensional external flow have been thoroughly investigated and reported in various literature. Although there is always room for some improvement, particularly in the modelling of the convective heat transfer coefficient, it is considered likely that significant further

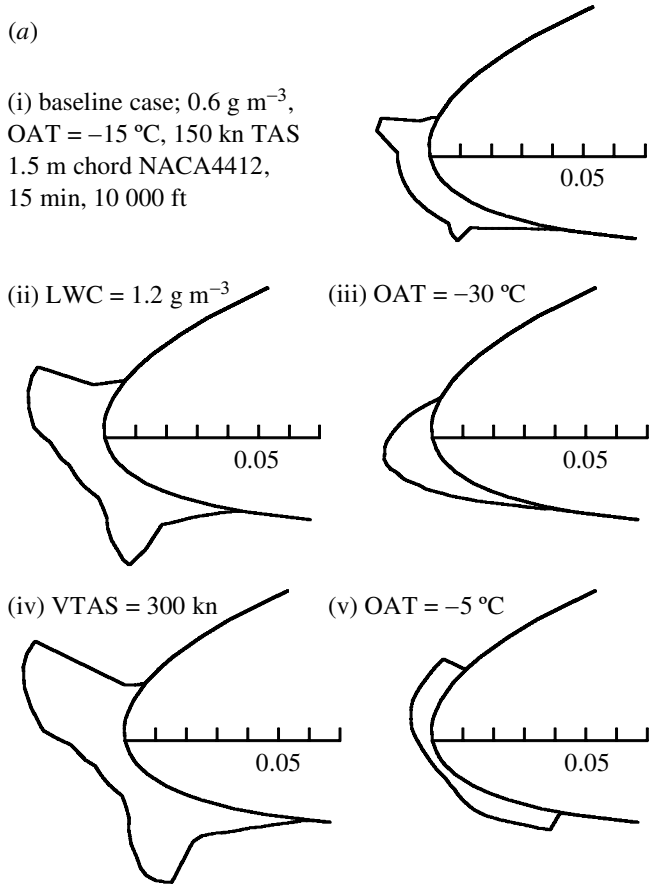

Figure 13. (*a*) Illustration of the effect of key parameters on the ice-accretion profile.

progress can only be realized after the Messinger based methods of today, employing control volume techniques, are replaced by methods which represent more closely the microphysical properties of the ice. This is likely to require analysis of the freezing of individual droplets, the water film generation, transport and subsequent freezing to form a rough surface. This should lead to the prediction of localized three-dimensional features such as rime feathers, glaze nodules and so-called 'lobster-tail' ice which forms on highly swept wings.

For anyone wishing to develop their own ice-accretion prediction code, there is as yet no agreed database of ice shapes against which the accuracy of the code may be checked. However, the NATO-RTO-AVT-006 working group is currently addressing this issue.

It is considered that more research is required to validate ice-accretion codes for multi-element aerofoils, bodies of revolution and three-dimensional flow conditions. Codes for these applications are still less widely used within industry at this time.

Extension of the codes to model freezing rain and drizzle has commenced, but more research is required to fully validate them. This is likely to require additional test evidence.

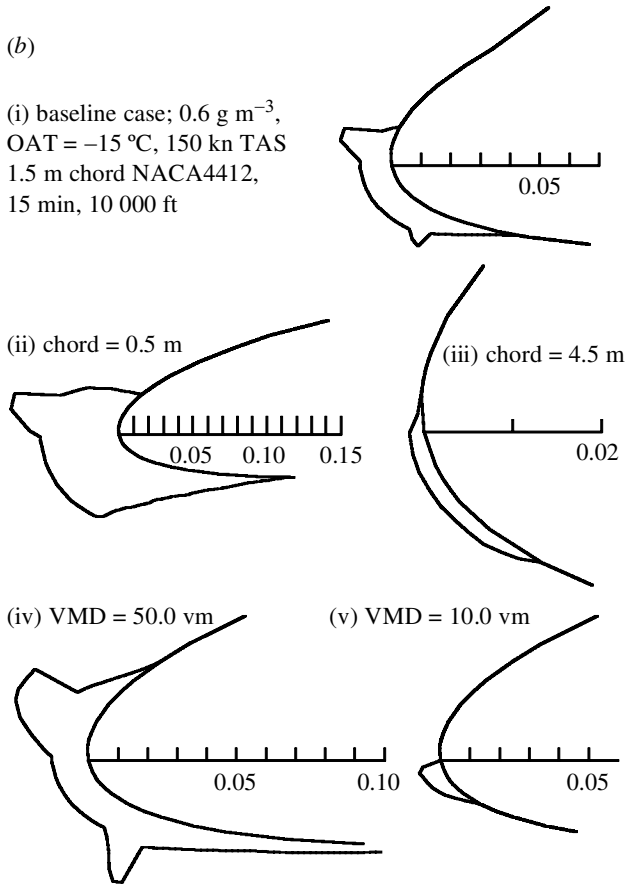

Figure 13. (*Cont.*) (*b*) Illustration of the effect of key parameters on the ice-accretion profile.

6. Performance degradation

(*a*) *Empirically based solutions*

The immaturity of CFD methods and the shear complexity of the theoretical analysis of iced aerofoil performance not surprisingly led early researchers to tackle the problem empirically. Gray (1964) produced a correlation for the aerodynamic penalties caused by ice accretion on wings of various section. However, this correlation proved only accurate when applied to the data on which it was based and could not therefore be applied more generally. More recent attempts by Flemming & Lednicer (1985) of Sikorsky, using NASA funding, considered a much wider range of parameters which were closely aligned to the needs of rotorcraft. These included relatively high Mach number ($M = 0.6$) and the effects of pitch oscillation which tended to reduce the level of profile drag increase. Correlations for lift, drag and pitching moment were subsequently checked against an extensive range of model rotor icing tunnel test data but a lack of data limited the range of comparisons with full size rotorcraft. The correlations included an expression for the onset of rotor icing and for spanwise extent. DERA believed these could be predicted by analysis and hence it was not necessary to rely on correlations for these aspects.

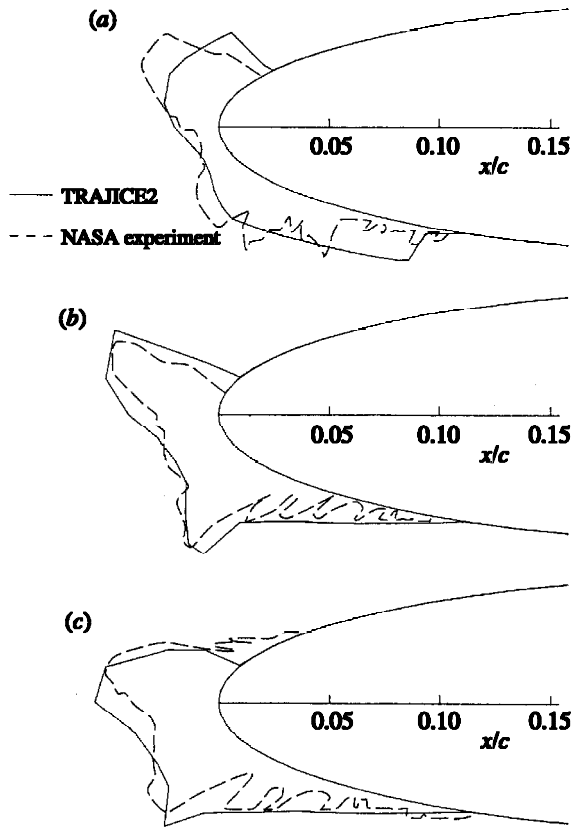

Figure 14. Example of typical spread in accuracy achievable with ice-accretion prediction codes. Incidence is 4°, airspeed is 94 m s^{-1}, VMD is 20 μm, LWC is 1.05 g m^{-3}, time is 6.2 min. (*a*) $t = -6.6$ °C; (*b*) $t = -12.2$ °C; (*c*) $t = -16.6$ °C.

With a need for aerodynamic performance data appropriate to RAE aerofoil sections, Gent & Beauchamp (1987) conducted tests in an icing wind-tunnel to record drag data for the traditional NACA 0012 rotorcraft aerofoil section along with a modern cambered design, RAE 9645. The results *inter alia* showed that the level of drag increase caused by rime, glaze and beak type ice was essentially the same for similar lifting conditions, at least for the 12% thickness-to-cord ratio aerofoils tested. Subsequently, Gent (1994*a*) produced a correlation which, in combination with additional data from the Sikorsky tests, was embedded into a rotor power required prediction model in order to estimate the performance of a helicopter with an unprotected rotor while flying in icing. Subsequent comparisons against NASA scale model data, and with full scale for a wide range of conventional helicopters, showed the trend with key atmospheric parameters could be predicted relatively well, although the magnitude of the power increase showed some scatter. The scatter was attributed to a combination of inaccuracies in the correlations, but also to the icing conditions, which are never constant during the encounter, requiring a mean value input to the code.

For fixed-wing aircraft, the empirical route to performance estimation continues to be aircraft specific. Model scale replicas of ice profiles, nowadays obtained using an ice-accretion prediction code, can be applied to scale models of aircraft. The measured

aerodynamic data are used both to confirm which areas require ice protection and, equally importantly, which areas may be left unprotected. The tests also help reduce the risk of icing flight trials, both with full-scale replica ice and in natural icing.

In all of the cases highlighted above, the goal has been, and largely remains, to be able to predict the aerodynamic performance data directly by analysis. The rapid advance over the last decade in CFD development has meant that complex codes are now routinely used and available to aircraft engineers. The next section therefore addresses this highly significant phase of the work.

(*b*) *Theoretically based solutions*

The performance degradation of aircraft in icing conditions can be assessed theoretically using CFD methods. Many types of CFD methods are now available. Those suitable for analysing the performance degradation of aircraft due to icing can be grouped into two categories as described in the following sections.

(i) *Coupled methods*

By coupling an inviscid flow solution with an integral boundary-layer calculation, the aerodynamic performance (lift and drag) of a wing or rotor can be obtained. A number of different approaches to this basic methodology have been used.

The inviscid flow solution could be obtained from a CFD code that solves the Euler equations, enabling compressibility effects to be modelled. However, since icing is usually a problem at low Mach numbers, a more popular method is to use a potential code. Panel methods (see, for example, Cebeci 1989) or finite-difference methods (see, for example, Collyer 1976) have been used to calculate potential flow solutions within coupled CFD codes. The pressures obtained by the inviscid flow solution are then used to calculate the boundary-layer development. The displacement effects of the boundary layer and wake are then fed back into the inviscid flow calculation, thereby coupling the viscous and inviscid elements of the code. An iterative procedure is then employed until a converged solution is obtained.

Coupled methods are computationally efficient and can be very accurate at predicting the aerodynamic performance of clean aerofoils. However, their iced aerofoil performance prediction capability is somewhat limited, owing to the inability of integral boundary-layer methods to model the regions of separated flow often associated with flow around iced aerofoils. Some further developments have been made to coupled methods to improve the modelling of small separated flow regions (see Cebeci 1989; Ashill *et al*. 1987), but the fundamental limitations of the boundary-layer theory usually make the codes impractical for general use with iced aerofoils.

Furthermore, coupled methods are unable to model stalled flow. Therefore, the maximum lift capability of an aerofoil cannot be evaluated using coupled methods.

(ii) *Navier–Stokes methods*

In view of the limitations associated with coupled methods, most iced aerofoil performance analysis is performed using Navier–Stokes CFD methods (see, for example, O'Brien 1996; Cantariti *et al*. 1998). CFD codes which solve the Reynolds averaged Navier–Stokes equations are able to implicitly model compressibility effects, viscous effects and are able to model separated flow regions. In addition, if the codes are

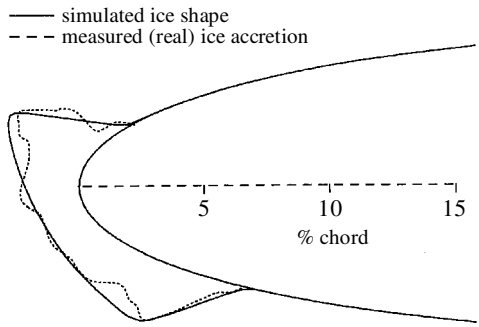

Figure 15. Comparison between the generic ice shape used for the CFD analysis and the real ice accretion on which it was based.

able to model unsteady flow behaviour (see, for example, Cantariti *et al*. 1998), the characteristics close to and beyond stall can be predicted, enabling the maximum lift capability to be evaluated.

However, the accuracy of the codes is largely dependent on the quality of the grid generated around the profile. Also, the choice of turbulence model used by code has an effect on accuracy. Furthermore, Navier–Stokes codes are computationally expensive when compared to other CFD methods.

(*c*) *Review of research*

A number of investigations have been performed to analyse iced aerofoil performance using CFD methods. Most of these investigations have studied the aerodynamic degradation of a NACA 0012 aerofoil with a generic ice shape (figure 15). This generic ice shape has the major characteristics of a glaze ice shape but without the irregularities.

(i) *BVGK*

BVGK (Ashill *et al*. 1987) is a coupled viscous/inviscid interaction solver which has a proven accuracy for computing transonic flow about clean aerofoils in two-dimensional flow. It has been used to predict the aerodynamic performance of both the clean and iced NACA 0012 aerofoils (see Dart & O'Brien 1996). Initially, the grid-generating element of the code could not map a grid around the complex geometry of the iced aerofoil. Modifications were made to the mapping routine, which allowed a grid to be generated but no solutions could be obtained using viscous flow. Solutions were obtained for inviscid flow, but the use of inviscid flow has little use in the prediction of the iced aerofoil drag.

Modifications to the geometry of the ice shape were attempted but still no useful predictions were obtained. It was therefore concluded that in its present form, the BVGK code is unsuitable for the prediction of iced aerofoil performance.

(ii) *N2DVC*

N2DVC (O'Brien 1996) is a Navier–Stokes flow solver developed by DERA for aerofoils in steady two-dimensional flow. Using the steady Reynolds averaged Navier–Stokes equations, and solving them with a finite-volume technique, steady flows can

be modelled. The results from this solver, as given in Dart & O'Brien (1996), were much more accurate than those from BVGK. However, at high incidences, due to the unsteady nature of the separation bubble aft of the ice accretion, converged solutions could not be obtained.

The unsteady nature of the flow prompted a similar investigation using an unsteady Navier–Stokes solver.

(iii) *PMB2D*

PMB2D (Cantariti *et al*. 1998) solves the unsteady Reynolds averaged Navier–Stokes equations using a pseudo-time formulation. The investigation reported in Allan (1998) found that the solutions obtained were very sensitive to grid quality. All calculations were performed using fully turbulent flow. This was necessary due to the occurrence of computational problems with the turbulence model (the linear k–ω model) when transitional flow was selected. The computational problems were speculated to be a result of the way the code models transition and it was therefore concluded that, in its present form, PMB2D is unsuitable for modelling iced aerofoils.

(iv) *Other research*

Apart from the good work reported by Potapczuk (1993), Cebeci (1989) and Habashi *et al*. (1998*b*), there appear to be relatively few data in the open press. However, DERA are privileged to have had sight of unpublished work conducted in industry by British Aerospace in the UK and Lockheed Martin in the US. The lack of publication reflects to some degree the relative immaturity of the work, although the main reason is the application to product specific tasks, which means that the results are proprietary, and publishing is counter to maintaining a commercial lead. The wide availability of Navier–Stokes solvers undoubtedly means similar tasks can be and probably are being undertaken more widely than appears at present.

For DERA at least, future research will be aimed at assessing different turbulence models, particularly Spalart–Allmaras (1994), with which NASA (Potapczuk 1993) has obtained very encouraging results.

7. Ice protection systems

Understanding where and at what rate ice will form on a body and knowing the effect of that ice on aerodynamic critical surfaces is, in reality, only the prerequisite to designing and certifying an ice-protection system. Though new forms of ice protection continue to be researched experimentally, most protection systems in use in aircraft today tend to be of more traditional design. Of these, hot-air and electrothermal methods have been analysed theoretically. In this section, only a very superficial review is provided, with the reader referred to more detailed information sources where these are available.

For large commercial transport aircraft, the thin metal surface and hollow leading edges lend themselves to protection using bleed air from the engines. The hot (*ca.* 200 °C) air is distributed in tubes along the wing and is sprayed from small holes onto the inner surface. The engine nacelles are usually protected in a similar way. The commercial pressures for fuel-efficient engines place great emphasis on minimizing bleed air mass flow. Hence the desire for a fully evaporative system

(more amenable to analysis) is not always achieved. Systems are usually designed to run wet in extreme icing conditions, while on other aircraft a de-icing approach may be adopted. Little information on codes appears to be available in the open press, although proprietary codes are known to be available within industry. British Aerospace have modified a version of the DERA TRAJICE2 code to include the internal heat transfer from impinging jets of hot air. A similar code has been developed by Fokker in Holland. Details of both codes are highly proprietary. Such codes require trajectory and ice-accretion analysis as described in the earlier sections. The codes known to DERA rely on empirical correlations for the internal heat transfer coefficient. The application of CFD to predict internal heat transfer appears to be in its infancy and offers good prospects for future research.

Electrothermal systems are usually confined to small areas such as intake lips, or to helicopter rotors. In parallel with development of ice-accretion prediction analysis, NASA, ONERA and DERA have developed codes for analysing both the one- and two-dimensional transient heat flow in a multi-layered structure with embedded electrical heating elements. A description of the codes and example results from two-dimensional codes may be found in Guffond *et al.* (1993). All of the codes are based on finite-difference methods applied in an energy balance formulation. The aim is to predict the new temperature within the structure after a small time-step, given the temperature within the structure at the start of the step. The calculation is repeated for as long as the analysis is required, i.e. many thousands of steps in practice. The choice of implicit or explicit formulations varies, but in any case the need for accuracy usually dictates the use of very small time-steps.

While Guffond (1983) and Beckett *et al.* (1988) solved the equations for the actual curved geometry, a comparison of results from the codes of NASA and DERA based on a 'flat-plate' analysis showed little advantage from analysing the more complex geometry. Accordingly, the simpler geometry continues to be analysed at present.

As with the codes for analysis of hot-air protection systems, electrothermal codes require water catch information from a trajectory analysis along with a knowledge of the basic external heat transfer mechanisms which remain the same as those considered for ice accretion. The main difference in relation to ice-accretion codes lies in the transient nature required of the analysis and the additional heat input term. The equilibrium temperature surface calculations of Messinger described earlier are therefore no longer appropriate. For de-icing systems, transient ice accretion and phase change must be considered. The thermal mass and diffusivity of the structure need to be taken into account.

NASA developed a 'staircase' approach to ice accumulation with ice accretion modelled as discrete blocks of ice. This approach was also adopted by DERA in its HRB2D code (see Gent 1995). Each block of ice may be in one of three states: all water, all ice or mixed ice/water at the phase change temperature. Ice phase change is normally approximated using an equivalent enthalpy method, which assumes the phase change occurs over a finite temperature interval (say, 1 °C), which allows an equivalent specific heat capacity to be established. The specific heat of the blocks within the staircase is therefore modified according to the temperature and degree of melting or freezing present. Some codes, such as that developed by DERA, include crude approximations for ice shedding.

The accuracy of the codes was demonstrated in Guffond *et al.* (1993) and, in the case of the DERA code due to Gent (1995), has been checked by comparisons with

data from both rig and flight test. The DERA code is now used in industry, including GKN Westland Helicopters Ltd.

8. Conclusions and future research recommendations

Though considerable progress has now been made in the field of aircraft ice-accretion and protection system analysis, there is nevertheless room for continued improvement.

In the case of ice-accretion analysis, prediction of the roughness of the ice and a more microscopic, rather than global, energy balance is required. At present, most, but not all, codes rely on the roughness being input to the code, even if based on an empirical correlation. The surface detail available from analysis at best reveals the main features (size and position of horns). It lacks the fine detail of localized roughness and rime feathers that form aft of the main accretion. Similarly, more research is required into the prediction of ice accretion on aerofoils approaching stall. This will undoubtedly dictate the use of more advanced Navier–Stokes flow solvers. There is evidence to suggest that the assumption that all impacting water remains on the surface is inaccurate, particularly for high values of LWC. More research is therefore required into droplet splash, and this may well involve the further development of the emerging water film models currently under development by Myers & Hammond (1999) and Habashi *et al.* (1998*a*).

References

Achenbach, E. 1977 The effect of surface roughness on the heat transfer from a circular cylinder to the cross flow of air. *Inst. J. Heat Mass Transfer* **20**, 359–369.

AGARD 1997 (Advisory Group for Aerospace Research & Development) Ice accretion simulation. Report of Fluid Dynamics Panel Working Group 20. NATO report AGARD-AR-344, December 1997.

Allan, M. R. 1998 Application of PMB2D unsteady Navier–Stokes solver for estimation of iced aerofoil performance. DERA/MSS/CR980544, October 1998.

Ashill, P. R., Woods, R. F. & Weeks, D. J. 1987 An improved semi-inverse version of the Viscous Garabedian and Korn method (VGK). RAE TR87002, January 1987.

Bartlett, P. 2000 Development of a new model of ice accretion on aircraft. In *9th Int. Workshop on Atmospheric Icing of Structures (IWAIS 2000), 5–8 June, Chester, UK.*

Beckett, P. M., Mousavi, A., Poots, G. & Gent, R. W. 1988 Mathematical model of an electrothermal de-icing system for a helicopter rotor. Part 2. Two-dimensional transient solutions. *Math. Engng Ind.* **2**, 19–49.

Bidwell, C. S. & Mohler Jr, S. R. 1995 Collection efficiency and ice accretion calculations for a sphere, a swept MS(1)-317 wing, a swept NACA 0012 wing tip, an axisymmetric inlet and a Boeing 737-300 inlet. In *33rd Aerospace Sciences Meeting and Exhibit, Reno, NV, USA, 9–12 January*, AIAA paper 95-0755.

Bidwell, C. S. & Potapczuk, M. G. 1993 Users manual for the NASA Lewis three-dimensional ice accretion code (LEWICE3D). NASA TM 105974, December 1993.

Cansdale, J. T. & Gent, R. W. 1983 Ice accretion on aerofoils in two-dimensional compressible flow: a theoretical model. Royal Aircraft Establishment Technical Report 82128, January 1983.

Cantariti, F., Badcock, K. & Gribben, B. 1998 Theory guide to PMB2D Version 3.0, July 1998. Aerospace Engineering Department, University of Glasgow.

Caruso, S. C. 1994 Three-dimensional unstructured mesh procedure for iced wing flowfield and droplet trajectory calculations. In *32nd AIAA Aerospace Sciences meeting, 10–13 January, Reno, NV, USA*, AIAA paper 94-0486.

Cebeci, T. 1989 Calculation of flow over iced airfoil. *AIAA J.* **27**, 853–861.

Collyer, M. R. 1976 A user guide to a program for computing viscous transonic flows past aerofoils. RAE Technical Memorandum Aero 1693, September 1976.

Dart, N. P. 1995 TRAJICE3D: a water droplet trajectory prediction program for wings and other three-dimensional bodies. Defence Research Agency, DRA-AS-STD-WP95133-1, August 1995.

Dart, N. P. & O'Brien, P. 1996 Analysis of iced aerofoil performance using CFD codes—current status. DERA/AS/ASD/CR96375/1, December 1996.

Flemming, R. J. & Lednicer, D. A. 1985 Correlation of airfoil icing relations ships with two-dimensional model and full scale rotor test data. In *AIAA 23rd Aerospace Science Meeting, 14–17 January, Reno, NV, USA*.

Gent, R. W. 1984 Calculation of water droplet trajectories about an aerofoil in steady, two-dimensional, compressible flow. RAE Technical Report 84060.

Gent, R. W. 1994*a* An empirically based method for the prediction of helicopter power increase during flight in icing weather conditions. DRA-AS-STD-WP94025/1.

Gent, R. W. 1994*b* TRAJICE2: a combined water droplet and ice accretion prediction code for aerofoils. RAE Technical Report 90054.

Gent, R. W. 1994*c* SPINNICE: a combined water droplet trajectory and ice accretion prediction program for spinners and similar axisymmetric bodies. Defence Research Agency, DRA-AS-STD-WP94055-1, March 1994.

Gent, R. W. 1995 HRB2D: a computer program for the detailed design and assessment of electrothermal rotor ice protection systems. Defence Research Agency Technical Report DRA/AS/STD/TR95027/1, June 1995.

Gent, R. W. & Beauchamp, A. R. 1987 Measurement of drag increase due to ice accretion on aerofoils of NACA0012 and RAE9645 section. RAE Technical Report 87013.

Gent, R. W., Markiewicz, R. H. & Cansdale, J. T. 1987 Further studies of helicopter rotor ice accretion and protection. *Vertica* **11**, 473–492.

Gent, R. W., Berkowitz, B. M., Guffond, D. & Reinmann, J. J. 1993 DRA/NASA/ONERA collaboration on icing research. Part I. Droplet trajectory calculations. Defence Research Agency Technical Report DRA/MS/TR93085/1, December 1993.

Gent, R. W., Rowley, D. J., Curtis, R. K. & Talbot, N. 1996 Advisory material for helicopter limited icing clearances. CAA Paper 96009, December 1996.

Gray, V. H. 1964 Prediction of aerodynamic penalties caused by ice formation on various aerofoils. NASA TN D2166.

Guffond, D. 1983 Programme de simulation numerique d'un degivreur electrique de bord d'attaque de voilure. Rapport Technique ONERA No. 13/5146 SY.

Guffond, D. & Brunet, L. 1985 Validation du programme bi-directional de caption. ONERA RT 20/5146.

Guffond, D., Henry, R., Reinmann, J. J., Wright, W. & Gent, R. W. 1993 NASA/ONERA/DRA collaboration on icing research. Part III. Electrothermal de-icing system modelling. ONERA Technical Report 2/7766 PN, June 1993.

Habashi, W. G., Bourgault, Y., Beaugendre, H., Lepage, C. Y. & Croce, G. 1998*a* FENSAP-ICE: a new equilibrium model for ice accretion, including film runback and conjugate heat transfer. In *ECCOMAS 98*, vol. 1, pp. 723–728. Wiley.

Habashi, W. G., Bougault, Y., Baruzzi, G. S., Boutanios, Z., Croce, G. & Wagner, W. A. 1998*b* FENSAP-ICE: an integrated CFD approach to the in-flight icing problem. In *ECCOMAS 98*, vol. 2, pp. 512–517. Wiley.

Hammond. D. W. 1998 Report on microstructure of impact ice. British Aerospace (Operations) Ltd, report for DTI contract RA/6/31/05, ICECREMO/REP/BAE/DWH/980312/1, March 1998.

Hansman, R. J. 1984 The effect of the atmospheric droplet size distribution on aircraft ice accretion. AIAA paper 84-0108.

Hardy, J. K. 1946 Protection of aircraft against ice. RAE Report SME 3380.

Hedde, T. & Guffond, D. 1993 Improvement of the ONERA 3D icing code, comparison with 3D experimental ice shapes. In *31st AIAA Aerospace Sciences meeting, 11–14 January, Reno, NV, USA*, paper AIAA 93-0159.

Kays, W. M. & Crawford, M. E. 1980 *Convective heat and mass transfer*, 2nd edn. McGraw-Hill.

Kim, J. J. 1986 Particle trajectory computation on a 3-dimensional engine inlet. NASA CR 175023, January 1986.

Langmuir, I. & Blodgett, K. B. 1946 A mathematical investigation of water droplet trajectories. Army Air Forces Technical Report 5418.

Lozowski, E. P. & Oleskiw, M. M. 1983 Computer modelling of time-dependent rime icing in the atmosphere. CRREL Report 83-2, January 1983.

Mason, B. J. 1971 *The physics of clouds*. Oxford Monographs on Meteorology, 2nd edn, p. 594. Oxford: Clarendon.

Meijer, S. 1987 Computation of rime ice accretion on airfoils. The Aeronautical Research Institute of Sweden. FFA TN 1987-08.

Messinger, B. L. 1953 Equilibrium temperature on an unheated icing surface as a function of airspeed. *J. Aeronautical Sci.* **20**, 29–41.

Mingione, G., Brandi, V. & Saporiti, A. 1999 A 3D ice accretion simulation code. In *37th AIAA Aerospace Sciences Meeting & Exhibit, 11–14 January, Reno, NV, USA*, AIAA paper 99-0247.

Ministry of Defence 1987 General specification for aircraft gas turbine engines. Defence standard 00-971.

Ministry of Defence 1994 Defence and airworthiness requirements for service aircraft. Defence standard 00-970, chapter 711, amendment 10.

Myers, T. G. & Hammond, D. W. 1999 Ice and water film growth from incoming supercooled droplets. *Int. J. Heat Mass Transfer* **42**, 2233–2242.

O'Brien, P. 1996 An accurate and robust methods for calculating viscous flows: final report. DRA/AS/ASD/CR/96120/1.

Potapczuk, M. G. 1993 Ice accretion and performance degradation calculations with LEWICE/NS. In *31st AIAA Aerospace Sciences Meeting & Exhibit, 11–14 January, Reno, NV, USA*, AIAA paper 93-0173.

Roach, W. T., Forrestor, D. A., Crewe, M. E. & Watt, K. F. 1984 An icing climatology for helicopters. Meteorological Office Special Investigations Memorandum 112.

Ruff, G. A. 1999 Automated comparison of ice accretion shapes. In *37th AIAA Aerospace Sciences Meeting & Exhibit, 11–14 January, Reno, NV, USA*, AIAA paper 99-0625.

Smith, A. G. & Spalding, D. B. 1958 *J. R. Aeronautical Soc.* **62**, 60–64.

Spalart, P. R. & Allmaras, S. R. 1994 A one-equation turbulence model for aerodynamic flows. *Recherche Aerospatiale* **1**, 5–21.

Tan, J. 1991 RAMP_VAX: a computer code to predict dust separation or ice accretion in gas turbine intakes. Cranfield Institute of Technology, UK, January 1991.

Wright, W. B. 1995 Users manual for the improved NASA Lewis ice accretion code LEWICE 1.6. NASA CR 198355.

Wright, W. B., Gent, R. W. & Guffond, D. 1987 General specification for aircraft gas turbine engines. Defence standard 00-971.

Wright, W. B., Gent, R. W. & Guffond, D. 1997 DRA/NASA/ONERA collaboration on icing research. Part II. Prediction of airfoil ice accretion. NASA CR 202349, May 1997.